RHIC Beam Use Request For Runs 11 and 12

The STAR Collaboration
June 4th, 2010

Table of Contents

RHIC Beam Use Request
For Runs 11 and 12

The STAR Collaboration

June 4th, 2010

1.   Executive Summary

The STAR Collaboration makes the following two-year beam-use proposal, in order to achieve its spin and relativistic heavy ion physics goals on a timescale consistent with intense international interest and competition in these areas, as well as to utilize RHIC beams effectively, taking full advantage of planned improvements in machine and detector capability as a function of time:

Run	Energy	Time	System	Goal
11[(1)]	$\sqrt{s_{NN}}$ = 18, 27 GeV	2 weeks	Au + Au	100, 150M minbias
	$\sqrt{s_{NN}}$ = 200 GeV	4 weeks	U + U	200M minbias 200M central
	$\sqrt{s}$ = 500 GeV[(a)]	5 weeks 6 weeks	$p_\uparrow p_\uparrow$ $p_\rightarrow p_\rightarrow$	trans. $P^2*\mathcal{L}$= 4 pb^{-1} long. $P^2*\mathcal{L}$= 20 pb^{-1}
		1 week	$p_\uparrow p_\uparrow$	pp2pp at high β*
12[(2)]	$\sqrt{s}$ = 500 GeV[(b)] or $\sqrt{s}$ = 200 GeV[(c)]	10 weeks	$p_\rightarrow p_\rightarrow$ or $p_\uparrow p_\uparrow$ $p_\rightarrow p_\rightarrow$	long. $P^2*\mathcal{L}$= 50 pb^{-1} $P^4*\mathcal{L}$= 15 pb^{-1} or trans. $P^2*\mathcal{L}$= 8.5 pb^{-1} long. $P^4*\mathcal{L}$= 4.3 pb^{-1}
	$\sqrt{s_{NN}}$ = 200 GeV	10 weeks	U + U Au+Au	3.5 nb^{-1} 5 nb^{-1}

Table 1.1: STAR Beam Use Request for Runs 11 and 12.

(1) 25 cryo weeks, 18 weeks production with three species
(2) 25 cryo weeks, 20 weeks production with two species.

(a) 50% or higher polarization in both yellow and blue rings should be routinely achieved towards the end of this run.

(b) Contingent on 50% or higher polarization in both yellow and blue beams. This request is part of the multiyear $\sqrt{s}$ = 500 GeV program to sample 300 pb^{-1} with 70% beam polarization.

(c) Request is to complete the Run 9 spin physics goals at $\sqrt{s}$ = 200 GeV. This request will move to Run 13 if sufficient polarization is achieved at 500 GeV during Run 11 to continue 500 GeV collisions during Run 12.

In this proposed physics-driven plan, the STAR Collaboration intends to make the most efficient use of RHIC beam time and upgrades in order to make timely progress in determining the QCD phase structure within the reach of RHIC, the properties of the new state of matter produced at top RHIC energy, to map the x dependence of the gluon polarization in the proton, $\Delta g(x)$, and to delineate the polarizations of the light quark and anti-quarks in the proton, $\Delta q(x)$, by flavor.

The primary goals of the proposed program are:

Run 11: 25 cryo-weeks, 18 weeks for physics production with three species*:

a) Two weeks: Search for the existence and location of the QCD Critical point. Complete the Phase-I Beam energy Scan (BES) program at RHIC. This includes the two remaining beam energies: $\sqrt{s_{NN}}$ = 18 GeV and 27 GeV Au+Au collisions.

b) Four weeks: 200 GeV U+U collisions, in order to study in more detail the properties of matter produced at top RHIC energy.

c) Eleven weeks: First characterization of transverse spin physics asymmetries at $\sqrt{s}$ = 500 GeV and continue statistically significant measurement of the parity violating longitudinal single spin asymmetry, A_L, in W$^-$ production at mid-rapidity. This program requires five weeks of transversely polarized and six weeks of longitudinally polarized $\sqrt{s}$ = 500 GeV p+p collisions.

d) Continue the pp2pp program begun in Run 9, with transversely polarized beams, for studies of diffractive physics and search for glueballs at central rapidity.

Run 12: 25 cryo-weeks, 20 weeks for physics production with two species:

a) Ten weeks: First physics production run after the completion and installation of the Forward GEM Tracker (FGT) for the measurement of the parity violating single spin asymmetry, A_L, in W production at forward-rapidity and of gluon polarization, $\Delta g(x)$, at $\sqrt{s}$ = 500 GeV. This program requires longitudinally polarized p+p collisions at $\sqrt{s}$ = 500 GeV and aims, in several years of running, to sample a total of 300 pb^{-1} with 70% beam polarization.

b) Ten weeks: In Run 12, we request to return to high luminosity heavy ion running to take full advantage of envisioned improvements in stochastic cooling. We expect that the pp-equivalent luminosity for Au+Au and U+U will be similar, so the choice of whether to request high luminosity U+U or Au+Au will be driven by results seen from the commissioning of U+U in Run 11.

* We would support additional test on $\sqrt{s_{NN}}$ = 5 GeV Au+Au collisions in Run11 as needed by C-AD.

2.   Report on Run 10 Performance and Progress on Data Analysis

2.1.   Introduction

The main physics goals for Run 10 were twofold. First was to obtain a large sample of 200 GeV Au+Au collisions with completed, full azimuthal coverage, Time-of-Flight and DAQ1000 upgrades. Since the SVT detector and associated support structures have been removed, this run has minimal material in the STAR detector, and so is optimized for electron and di-electron measurements. Second, to begin the Beam Energy Scan (BES) program to search for the existence and the location of the QCD phase boundary and the possible critical point. Phase-I of the BES will cover the energy range $\sqrt{s_{NN}} = 39 - 7.7$ GeV, along with a test from C-AD of collisions at $\sqrt{s_{NN}} = 5$ GeV. In sections 2.2 and 2.3, we discuss Run 10 performances. In Sections 2.4 and 2.5, we discuss some selected analysis highlights from the STAR experiment.

2.2.   Run 10 Detector Performance and Statistics

In Run 10, the STAR detectors were positioned to take data for top energy Au+Au collisions and the Phase-I BES program at different energies. Table 1 shows the changes/upgrades to the detectors and their electronics. The new additions are the fully complete Time-of-Flight Detector, a new Trigger-Clock Unit (TCU), online tracking on every event by a high-level trigger (HLT), and rework of the readout electronics of the Barrel EMC Shower-Maximum Detector.

Component	**TOF** Time-of-Flight Detector (% installed)	**FTPC+PMD** Forward TPC Photon-Multiplicity Detector	**TCU** Trigger-Clock Unit	**BSMD** Barrel EMC Shower-Max Electronics	**FMS** Forward Meson Spectro-meter	**HLT** High-Level Trigger
Physics	Dilepton, PID correlation and fluctuation	Reaction Plane, Flow, DCC	General	Jet, Heavy-flavor	CGC, Transverse Spin	High-p_T, J/Ψ, Exotic
Run 9 p+p	75%	OFF	16bits	15% dead-time @300Hz	ON	test
Run 10 200 BES	100%	ON Repairs of PMD electronics	128bits	15% dead-time @600Hz	OFF	Online tracking on, every event

Table 2.1: Comparison of Detector configuration in Run 9 and Run 10.

The completion of the Time-of-Flight detector enables STAR to do particle identification along with the 2π TPC acceptance for major physics goals: dileptons, identified particle correlation and fluctuations, and the net-proton Kurtosis Analysis. The typical preliminary values of the TOF timing resolution are given in Table 2.2 for some of the energies for which STAR took data in Run 10. Also shown is the timing resolution at 39 GeV from a scheme without using the start time from the forward upVPD and using PID information from the STAR TPC. This is particularly useful for the lower beam energy program where due to the changing rapidity acceptance the upVPD has lower efficiencies for central collisions. The TOF timing resolution is at 85-90 ps, meeting our physics requirements.

Beam energy (GeV)	Timing Resolution (*ps*)	Remarks
200	85	
62.4	90	
39	86	Using a new calibration scheme without information of start time from VPD, 87 *ps* of timing resolution has been achieved

Table 2.2: TOF timing resolution in Au+Au collisions in Run 10.

The new Trigger-Control Unit increased trigger flexibility in trigger definitions and avoids packing different physics triggers into a single bit. The reduced dead-time of the BSMD increases the maximum bandwidth for full BSMD readout, which is a critical detector component for suppression of backgrounds in the electron channel. In Run 9, a substantial fraction of the triggers ran without BSMD readout, which avoided dead-time but also prevented its use in those trigger streams. In Run 10, the BSMD was read out in essentially every event, greatly improving the efficiency for the heavy-flavor program (Non-photonic electrons, J/Psi and Upsilon).

A High-Level trigger was deployed this run with online tracking on every triggered event from Level 0. The 24 Sector Level 3 (SL3) machines, which are used for the TPC data acquisition and cluster finding, are also used in sector-by-sector tracking. Tracks, tower information from the BEMC detector, time of flight from the TOF detector, and in the future, information from the HFT and MTD, are sent to Global Level 3 (GL3) machines, in which the complete event is reconstructed and a trigger decision is made. During Run 10, after the goals for minimum-bias and central collision events were reached, the HLT acted as a trigger decision in selecting interesting events to record.

 At higher beam energies, the HLT had three trigger components: high-p_T charged particle selection, J/Psi, and Heavy Nuclei with charge $|q|>=2$. During the BES, HLT served as an online monitoring device to reconstruct good collision events from large background (usually 1—10% of events taken are good collisions at $\sqrt{s_{NN}} = 7.7$ GeV). This role was crucial for the BES program; for more details we refer to BES section of this document.

STAR's data-taking efficiency was greatly improved over the last two years with DAQ1000, reduced dead-time in other detectors, and constantly improving data-taking

procedures. Some quantitative measures for how efficiently STAR ran for the 200 GeV portion of Run 10 are:

a) Fraction of time while luminosity was being delivered that STAR was taking data: 74%.
b) Overall fraction of the delivered luminosity sampled by STAR: 61%, though for many fills approaching 80%
c) Average live-time of all STAR detectors: 83% (mostly due to a choice to run the BSMD at high rates)
d) Loss of delivered luminosity at the beginning of a fill before the start of STAR data-taking: 12%
e) Delivered beam used for detector commissioning and losses due to other issues: less than 16%.
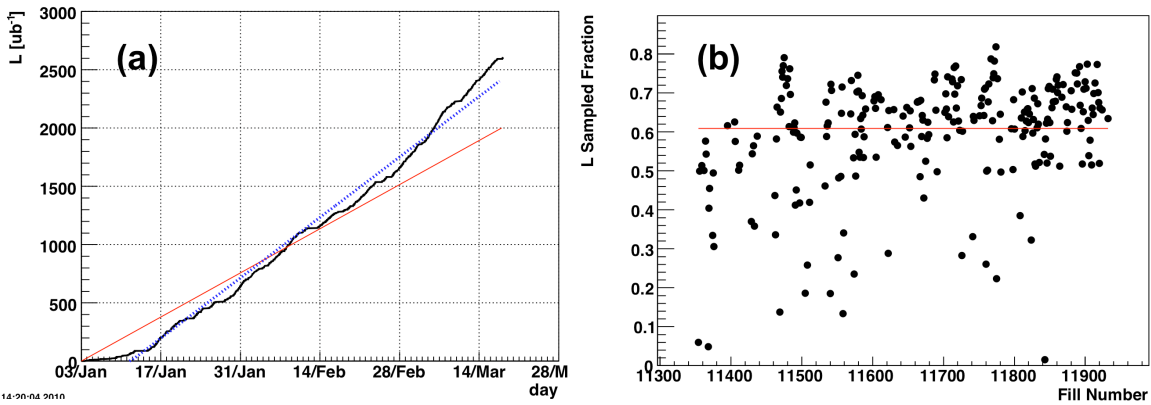
Figure 2.1: STAR Detector performance in 200 GeV Au+Au collisions. (a) Integrated luminosity from EMC high-tower trigger as a function of time. The red line is the linear projection for the targeted goal, the black histogram is the actual tracking of the sampled luminosity, and the blue line is a linear fit (b) Fraction of the sampled luminosity over the delivered luminosity per fill.

This, combined with excellent accelerator performance, led to the datasets shown in Table 2.3.

Beam Energy ($\sqrt{s_{NN}}$, GeV)	Minbias (Million)	Central (Million)	High-Tower Sampled Luminosity	FTPC+PMD (Million)
200	355/300	265/250	2.6/2 (nb^{-1})	5/5
62.4	143/(N/A)	33/(N/A)	175(ub^{-1})/(N/A)	3.5/(N/A)
39	250/25		62/9 (ub^{-1})	23/5
11.5	$\geq 7.5/5$	N/A	N/A	
7.7	5/5	N/A	N/A	
5	Commissioning	N/A	N/A	

Table 2.3: Actual data taken and the STAR Run10 BUR requests.

2.3. RHIC Beam Energy Scan Run 10 Performance

The main physics goals for STAR experiment in the Beam Energy Scan Program were presented in detail in the last STAR BUR and described in a STAR Internal Note [1]. Below we very briefly recapitulate them. We also present recent developments since the last BUR, concerning the study of higher moments of net-protons to look for critical point fluctuations. This study, currently using data from 200, 62.4 and 19.6 GeV Au+Au collisions, underscores the need for completion of Phase-I of the BES program.

2.3.1. Physics Goals for Run 10

A: Search for signatures of a phase transition and a critical point. The particular observables that we have identified as the essential drivers of our run plan are:

(A-1) Elliptic & directed flow for charged particles and for identified protons and pions, which have been identified by many theorists as highly promising indicators of a "softest point" in the nuclear equation of state;
(A-2) Azimuthally-sensitive femtoscopy, which adds to the standard HBT observables by allowing the tilt angle of the ellipsoid-like particle source in coordinate space to be measured; these measurements hold promise for identifying a softest point, and complements the momentum-space information revealed by flow measurements;
(A-3) Fluctuation measures, indicated by large jumps in the baryon, charge and strangeness susceptibilities, as a function of system temperature – the most obvious expected manifestation of critical phenomena.

B: Search for turn-off of new phenomena already established at higher RHIC energies. QGP signatures are the most obvious example, but we define this category more broadly. If our current understanding of RHIC physics and these signatures is correct, a turn-off must be observed in several signatures, and such corroboration is an essential part of the "unfinished business" of QGP discovery. The particular observables that STAR has identified as the essential drivers of our run plan are:

(B-1) Constituent-quark-number scaling of v_2, indicating partonic degrees of freedom;
(B-2) Hadron suppression in central collisions as characterized by the ratio R_{CP};
(B-3) Untriggered pair correlations in the space of pair separation in azimuth and pseudo-rapidity, which elucidate the ridge phenomenon;
(B-4) Local parity violation in strong interactions, an emerging and important RHIC discovery in its own right, is generally believed to require de-confinement, and thus also is expected to turn-off at lower energies

In the BUR for Run 10, STAR proposed to run at $\sqrt{s_{NN}}$ of 5, 7.7, 11.5, 18, 27 and 39 GeV. In Run 10 we took data at $\sqrt{s_{NN}}$ of 7.7, 11.5, and 39 GeV. The details of the data taking and its impact on the proposed physics program are discussed below along with the C-AD performance. In section 3 we present our beam request for completion of Phase-I of the Beam Energy Scan program at RHIC in Run 11.

It is essential to complete the BES program Phase-I in Run 11, as there are many constraining factors for the optimal running of this program in the near future in STAR. These include the upcoming Heavy Flavor Tracker (HFT) and Forward GEM Tracker (FGT) subsystems, which will impact the future availability of both Forward Time Projection Chambers (FTPCs) – proven, existing, subsystems that provide information about the reaction plane needed for measuring the v_1 component of flow and considerably extend pseudo-rapidity coverage. By Run 12, the FTPCs will be removed to make room for the FGT. By 2013, a new 4-cm diameter beam pipe will be in place in STAR in preparation for the HFT. From the experience on RHIC performance at these low energies collected during the BES program in Run 10, this smaller beam pipe could have serious implications for the BES program, due to backgrounds from beam-pipe collisions. Therefore, we view Run 11 as a unique opportunity for completion of the exploratory Energy Scan.

2.3.2. Higher Moments of net-proton Multiplicity Distribution

The STAR experiment has recently developed a new observable, based on results at previous energies, which can be used to look for critical point fluctuations at RHIC.

The correlation length (ξ) diverges at the Critical Point (CP). ξ is related to various moments of the distributions of conserved quantities such as net-baryons, net-charge, and net-strangeness [2]. Finite size and time effects in heavy-ion collisions put constraints on the values of ξ. A theoretical calculation suggests $\xi \approx$ 2-3 fm for heavy-ion collisions [3]. It was recently shown that higher moments of distributions of conserved quantities, measuring deviations from a Gaussian, have a sensitivity to CP fluctuations that is better than that of variance (σ^2), due to a stronger dependence on ξ [4]. The skewness goes as $\xi^{4.5}$ and kurtosis (κ) goes as ξ^7. A crossing of the phase boundary can manifest itself by a change of sign of skewness as a function of energy density [4, 5]. Lattice calculations and QCD-based models show that moments of net-baryon distributions are related to baryon number susceptibilities [6]. The product $\kappa\sigma^2$, related to the ratio of fourth order to second order susceptibilities, shows a large deviation from unity near the CP [6]. Experimentally measuring event-by-event net-baryon numbers is difficult. However, the net-proton multiplicity distribution is measurable. Theoretical calculations have shown that net-proton fluctuations reflect the singularity of the charge and baryon number susceptibility as expected at the CP [7].

Figure 2.2 shows the energy dependence of $\kappa\sigma^2$ for net-protons, compared to several model calculations that do not include a CP. Also shown at the top of Figure 2.2 are the μ_B values corresponding to the various $\sqrt{s_{NN}}$. We have not observed any non-monotonic beam energy dependence. The results from non-CP models are constants as a function of $\sqrt{s_{NN}}$ and have values between 1-2. The result from the thermal model is exactly unity. Within the ambit of the models studied, the observable changes little with change in non-CP physics (such as collective expansion and particle production) at the various energies studied. From comparisons to models and the lack of non-monotonic dependence of $\kappa\sigma^2$ on $\sqrt{s_{NN}}$ studied, we conclude that there is no indication from our measurements for a CP [8]. Clearly the data taken in Run 10 and proposed in Run 11 will be crucial to bridge the gap in baryon chemical potential regions to search for the CP in the QCD phase diagram.
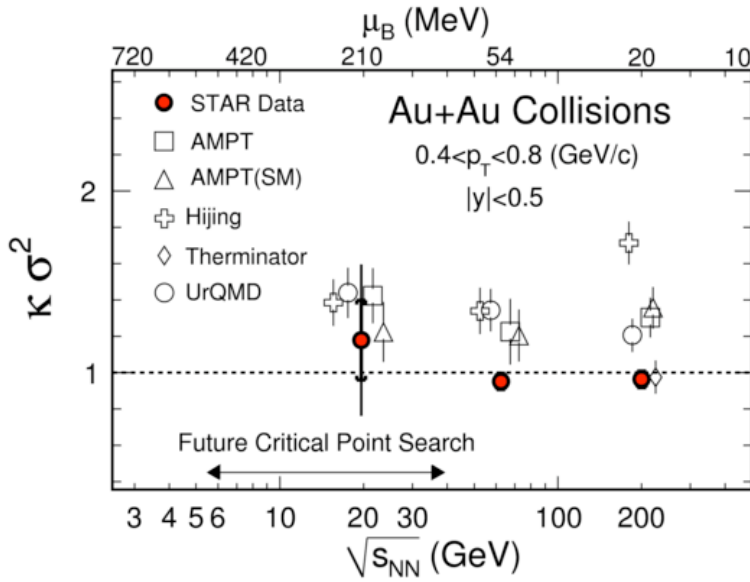
Figure 2.2: Energy and baryon-chemical potential dependence of $\kappa\sigma^2$ for net-protons, compared to several model calculations that do not include a CP. Experimental and model results are shown as filled symbols and open symbols, respectively. Figure taken from [9].

2.3.3. Data Quality from Run 10: 39 and 7.7 GeV Collisions in STAR and Impact on STAR Physics Program

STAR has completed the data taking for the allotted beam energies as the part of the Phase-I of beam energy scan program at RHIC in Run 10, as shown in Table 2.3 above. In order to achieve the physics goals for the beam energy scan program, it is important to verify the quality of the data taken. In this context we discuss below some key quality assurance plots for the 39 and 7.7 GeV data collected by STAR.
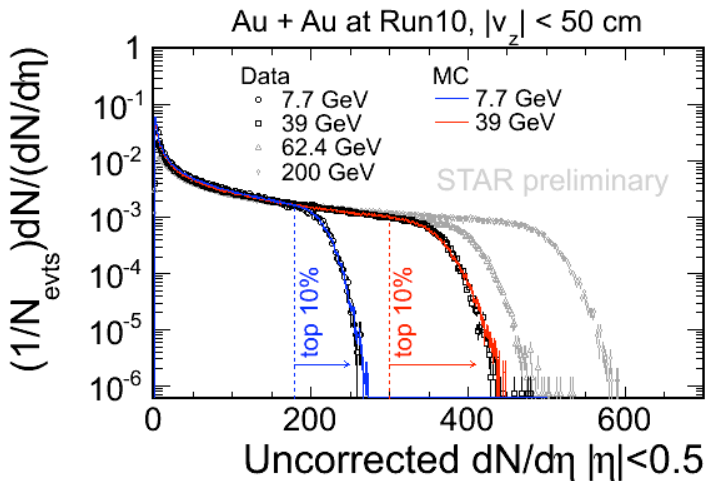

Figure 2.3: The uncorrected charged particle multiplicity distributions for the 39 and 7.7 GeV compared to higher energies of 62.4 and 200 GeV. A vertex cut $|v_z| < 50$ cm was applied for the plot.

Multiplicity Distribution: Figure 2.3 shows the uncorrected charged particle multiplicity distribution for the 39 and 7.7 GeV compared to higher energies of 62.4 and 200 GeV. The shape of the distributions at lower energies is comparable to that for the higher energies, with multiplicity being lower as the beam energy decreases. These distributions are

compared to Glauber model simulations to select the collision centrality. The top 10% central collisions are indicated. This shows STAR will be able to do a detailed centrality dependence study of various physics goals mentioned in the introduction from the Run 10 data set.

Particle Identification and Acceptance: In Run 10 the particle identification capabilities in STAR got a boost by the successful completion of the full barrel TOF. For physics analysis like those addressing NCQ scaling, fluctuations due to critical point and obtaining the freeze-out parameters it is important to have a good measurement of particle identification over the large acceptance in STAR.
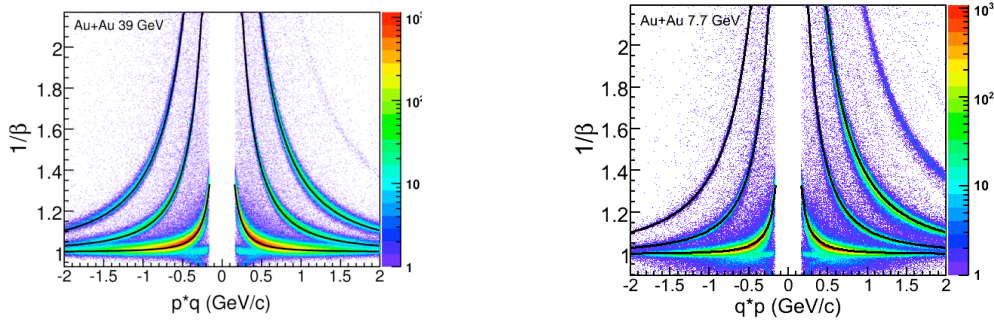
Figure 2.4: Particle identification with new barrel Time-of-Flight system. Left and right plots show the results from 39 GeV and 7.7 GeV collisions, respectively.

Figure 2.4 shows the enhanced particle identification capabilities with the TOF in STAR in Run 10 for Au+Au collisions at 39 and 7.7 GeV. The figure shows $1/\beta$ vs. rigidity. Comparing with the dE/dx distributions, in Figure 2.5 left and right for results from 39 GeV and 7.7 GeV, respectively, one can see that the momentum reach for identifying the various hadrons have significantly increased with the newly completed Time-of-Flight system in STAR.
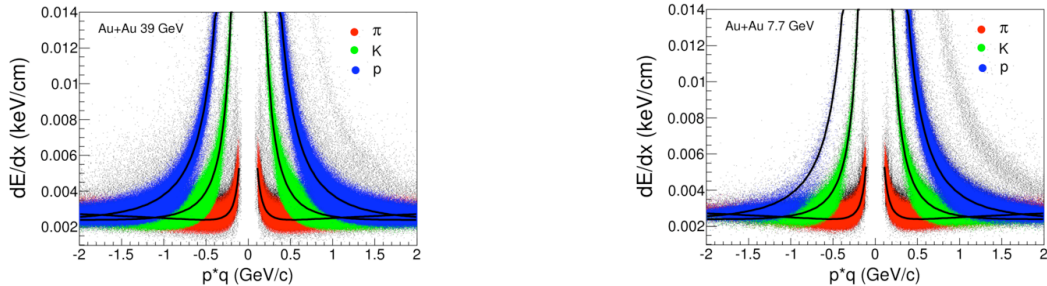

Figure 2.5: dE/dx vs. rigidity for different identified particles for the collisions at 39GeV (left) and 7.7GeV (right). The lines are theoretical expectations using Bischel functions.

One of the big advantages of experiments at RHIC compared to those at SPS is the uniform acceptance for each hadron species over all the beam energies studied. These can be seen from the rapidity vs. transverse momentum acceptance distributions below (Figure 2.6) for pion, kaon and proton, obtained using the STAR TPC+TOF at 7.7 GeV, 39 GeV and 200 GeV Au+Au collisions.

A common acceptance for identified hadrons at all beam energies is important for event-by-event type fluctuation studies and for interpretation of the physics results. These results show that the data taken by the STAR experiment can be used to deliver the physics goals related to studies using pions, kaons and protons.

Identified Particle Acceptance at STAR
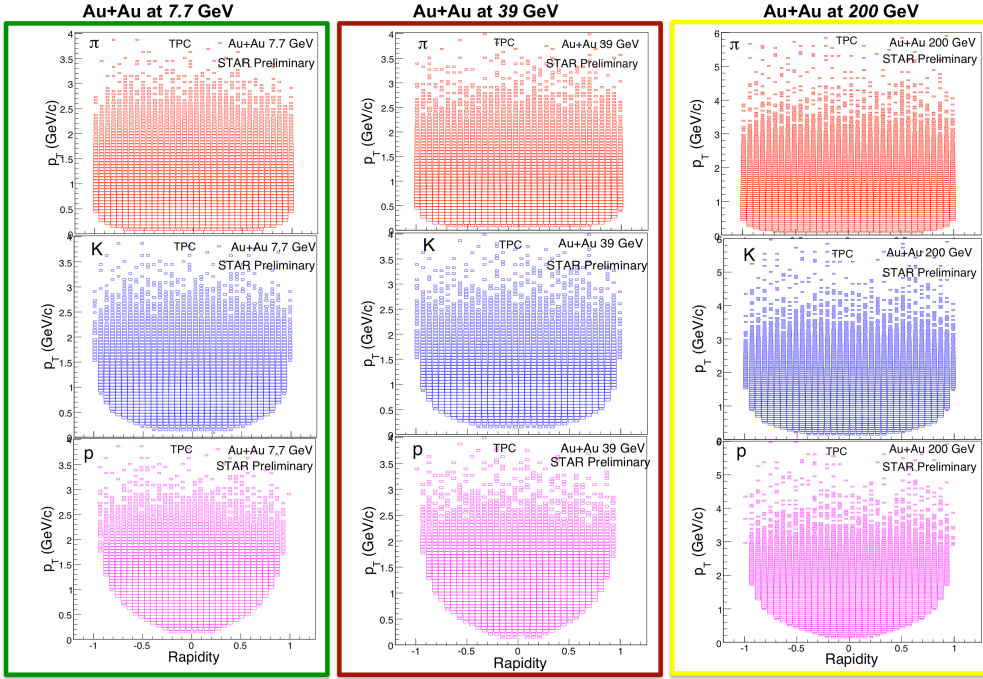
Figure 2.6: Acceptance in p_T vs. rapidity space for identified hadrons pions, kaons and protons from Au+Au collisions at 7.7 GeV (left column), 39 GeV (central column) and 200 GeV (right column). Although the beam energy has been varied over more than an order of magnitude, the acceptance for the identified hadrons do not vary.

Particle identification for topologically reconstructed hadrons is readily also available for Au+Au collisions for all beam energies at STAR. In Figure 2.7, we demonstrate the quality of the data (fast offline) taken through the accurate reconstruction of K_S, ϕ, Λ, Ξ, and Ω, using minimum bias data set for Au+Au collisions at 39 GeV. These hadrons are crucial to test onset of various interesting features observed at RHIC energies such as NCQ scaling in v_2 and suppression of high transverse momentum hadron production [10]. Added to this they will provide crucial information on energy dependence of strangeness enhancement.

Particle Identification at STAR
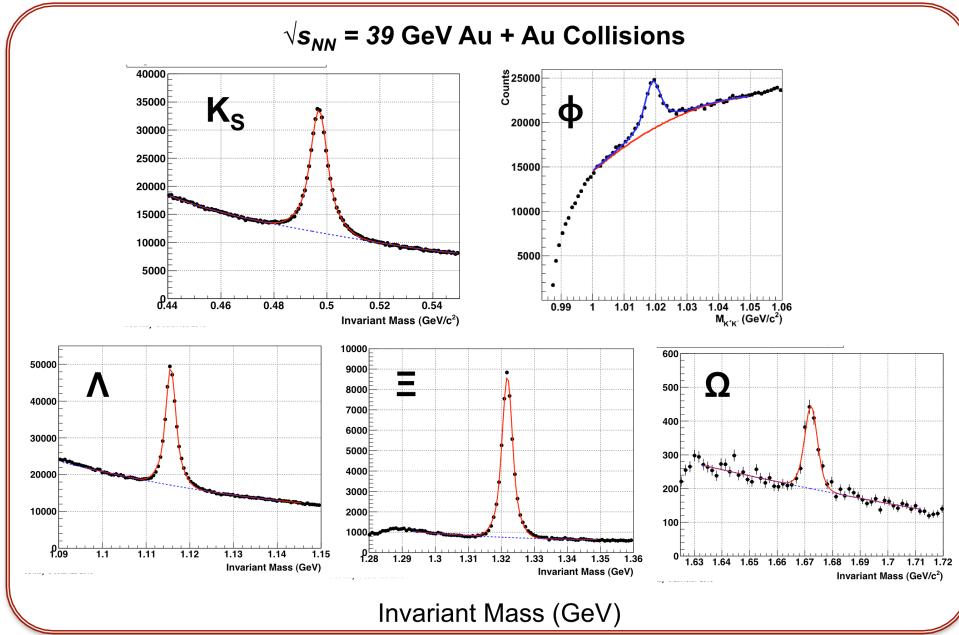
Figure 2.7: Topologically reconstructed hadrons: K_S, φ, Λ, Ξ, and Ω in Au+Au collisions at √s_NN = 39 GeV.

In order to demonstrate the quality of data from Run 10, we present preliminary results of the anti-proton over proton ratios for central Au+Au collisions versus collision energy in Figure 2.8. The red stars represent the preliminary data taken in Run 10 and black stars are those based on data collected by STAR in previous RHIC runs. The results show that STAR has been able to cover a significant region of the chemical potential range in the QCD phase diagram (approximately between $20 < \mu_B < 150$ MeV and $350 < \mu_B < 450$ MeV) up to Run 10. In the future, Run 11 will provide an opportunity to complete the required energies and event statistics to make the crucial measurements to search for evidence for the Critical Point and first-order phase transition. This could be done through the proposed running at beam energies of 18 and 27 GeV at RHIC.

Azimuthal Anisotropy and Event Plane Estimation: One of the crucial measurements for the BES program at RHIC is to study the baryon-meson dependence of azimuthal anisotropy as a function of hadron transverse momentum. In addition STAR plans to look into detail at v_1 measurements as a function of rapidity and azimuthally sensitive HBT measurements as a possible signature of phase transition. At these lower energies STAR will use the event plane information using detectors at forward rapidities while studying the anisotropy of hadron production at mid-rapidity. The forward detectors that will provide the event plane are the Forward Time Projection Chambers (for the higher energy end of the BES program, hence very crucial that the remaining part of the BES Phase-I gets completed in Run 11) and the Beam-Beam Counters. Preliminary investigations have shown that the Event Plane resolutions are sufficient to carry out the above physics goals. Results from TPC and FTPC are shown in Figure 2.9 for Au+Au collisions at 200, 39 and 7.7 GeV.
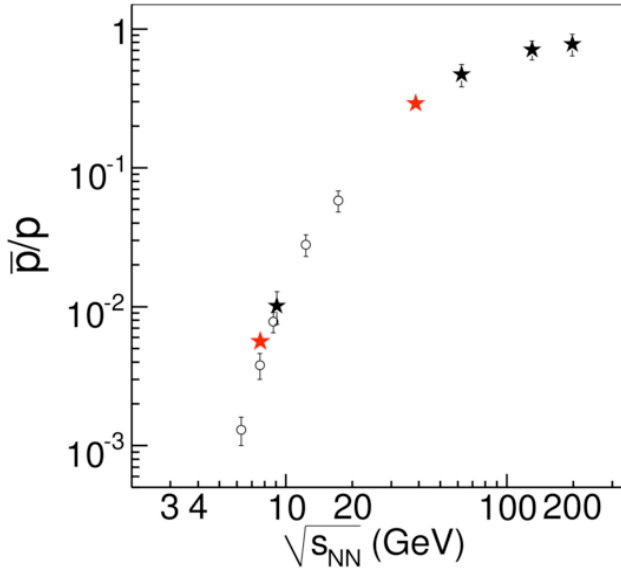
Figure 2.8: Anti-proton over proton ratios versus a function of the collision energy. Preliminary STAR results from $\sqrt{s_{NN}}$ = 7.7 and 39 GeV Au+Au central collisions are shown as red stars.
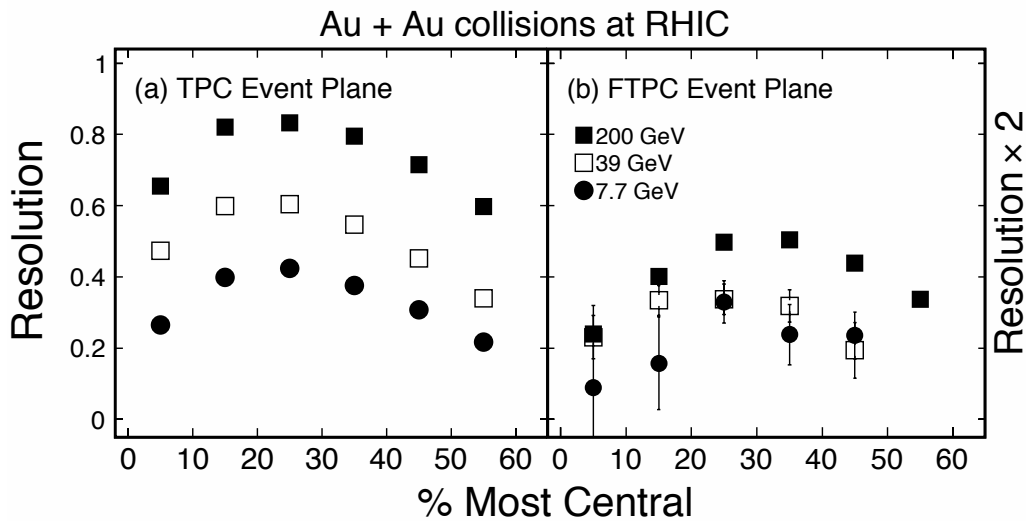
Figure 2.9: Event plane resolution for collisions at 200 GeV (filled squares), 39 GeV (open squares) and 7.7 GeV (filled circles). Preliminary results from 39 GeV and 7.7 GeV are from fast offline analysis. Left- and right-plots show the results from TPC and FTPC, respectively.

C-AD Performance for BES running at STAR: Figure 2.10(a) shows a sample for the average event rate in Hz in STAR for Au+Au collisions at 7.7 GeV. A clear increase in the event rate is observed after day 124, when the β^* in STAR was decreased to 6 m from 10 m around day 125. As one can see in Figure 2.10(b), the event rate was also enhanced when the length of the fill was reduced to 10 minutes. Average rates over the fill approached 8 Hz, as compared to the expectation of 3 Hz in the BUR for Run 10. This, along with an average time recording data of 14 hours/day, allowed the goal of 5M events to be reached in 5 weeks, rather than the 8 weeks that STAR requested in the Run 10 BUR.

14

Au + Au Collisions at 7.7 GeV
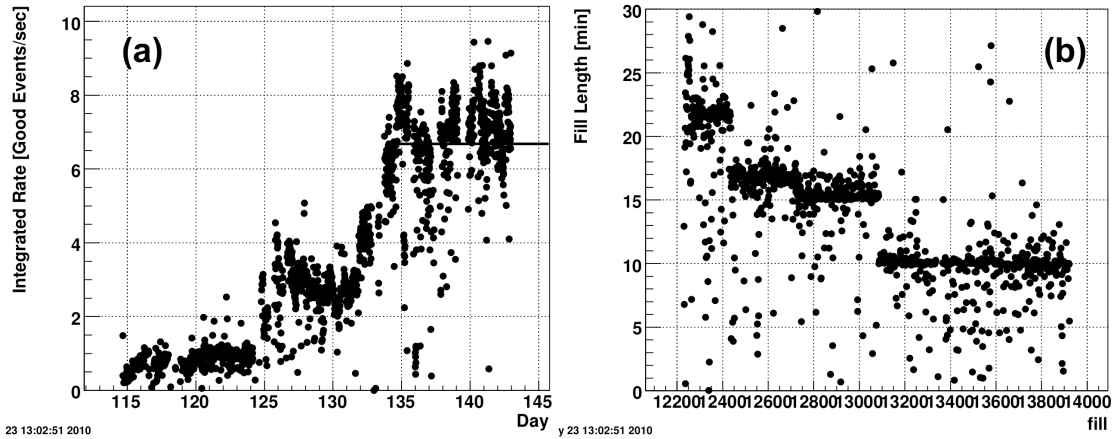
Figure 2.10 (a) Good events rate per fill; (b) Fill length. Clearly, the integrated rate is correlated with the filling length.

Figure 2.11 shows the side view (left plot) and beam view (right plot) of the collision points from a fast reconstruction of the tracks in STAR TPC. In the beam view plots, the outer red circle represents the approximate position of the beam pipe and the inner red circle corresponds to the radius of 2 cm on the plot. Events having this radii less than 2 cm are considered as good events in STAR for physics analysis. The plots clearly show that backgrounds from beam-beam pipe collisions are quite substantial in STAR at these low energies. The level of background was not constant, and could be reduced somewhat by tuning of the accelerator.
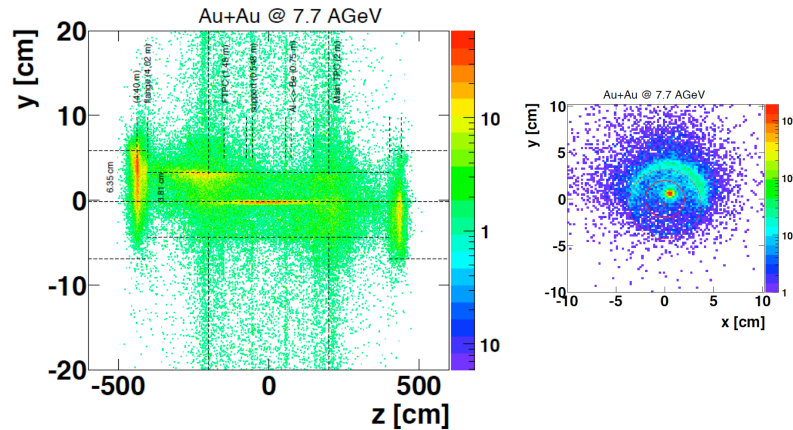
Figure 2.11: Beam tuning for 7.7 GeV Au+Au collisions, via primary vertex reconstruction offline. Various structures in the STAR detector, in which beam-structure collisions occur, are clearly visible in the x-y and y-z plots.

STAR employed a High-Level online tracker and Trigger (HLT), which collected information in real time from all detectors including the TPC, in order to estimate the number of good events during the BES program. The lower level L0 trigger was optimized

for efficiency rather than background rejection, since the event rate fit easily into the bandwidth available. Because of this, a cleaner signal was necessary for both accelerator-tuning and counting of events towards the physics goal. The core algorithm of the tracker in the HLT is a fast track finder based on conformal mapping. From these tracks, a 3-dimensional primary vertex position was reconstructed event-by-event online. The fraction of good events was then defined by those collected with a vertex radius of less than 2 cm, and was on the order of 3% for 7.7 GeV collisions. Figure 2.12 shows the Vertex X and Y distribution as reconstructed using the HLT in Au+Au collisions at 7.7 GeV. When compared to data reconstructed offline, the efficiency and purity of the HLT to tag good events were both approximately 95%.
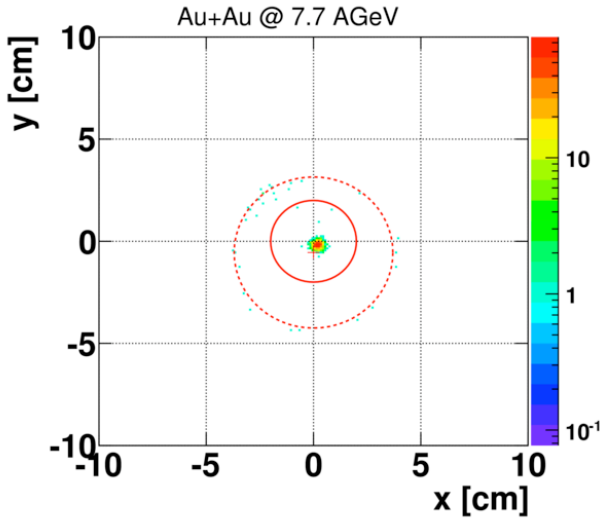
Figure 2.12: Beam position for good events determined by the STAR High Level Trigger (HLT).

2.4. Status of full-Jet Reconstruction in Au+Au Collisions at STAR

Full jet reconstruction in heavy-ion collisions can, in principle, provide a direct measurement of the energy of the scattered parton before energy loss, alleviating well know biases in di-hadron correlations and allowing reconstruction of parton kinematics in an unbiased way, independent of the fragmentation details (quenched or unquenched). This would result in a direct measurement of the energy loss probability distribution necessary to distinguish between different theoretical descriptions of partonic interactions with the hot QCD matter.

The current results from full-jet reconstruction at STAR (Y07) extend the kinematic reach of jet quenching measurements in central Au+Au collisions up to jet energies of ~40 GeV. Jet R_{AA} measurements suggest that, compared to single hadron measurements, with full jet reconstruction one is able to recover a larger fraction of the jet population (see Figure 2.13 left). The large acceptance of the STAR detector also allows the measurement of di-jets in the heavy-ion environment. By utilizing the high-tower (HT) triggered data-set one can select a surface-biased/unmodified trigger jet, thus enhancing the recoil jet population towards maximum path-length/modification, and can compare the di-jet coincidence rate with respect to p+p collisions (see Figure 2.13 right). In contrast to the minimum-bias

inclusive jet R_{AA} one observes a significant suppression in the di-jet coincidence, suggesting strong modifications in the jet structure due to partonic energy loss in the medium.

In order to quantify the modifications of the jet structure the ratio of the inclusive jet x-section, reconstructed with R=0.2 and R=0.4 in central Au+Au collisions, is shown in Figure 2.14 (left) where it is compared to p+p reference measurements. The differences suggest a significant broadening of the jet structure from 0.2 to 0.4 in central Au+Au collisions. This observation is also visible in the broadening of the recoil correlation functions in jet-hadron (as compared to di-hadron) correlations (see Figure 2.14 right). The advantage of this hybrid measurement, although it measures the broadening on a statistical and not jet-by-jet basis, is that it allows the quantification of the broadening beyond R=0.4, which in the case of full-jet reconstruction is currently limited due to fluctuations in the heavy-ion background. In Figure 2.14 (right) the background subtraction was approximated using a uniform background. The effect of elliptic flow and the corresponding uncertainties are still under investigation, but are not expected to change the qualitative conclusions.
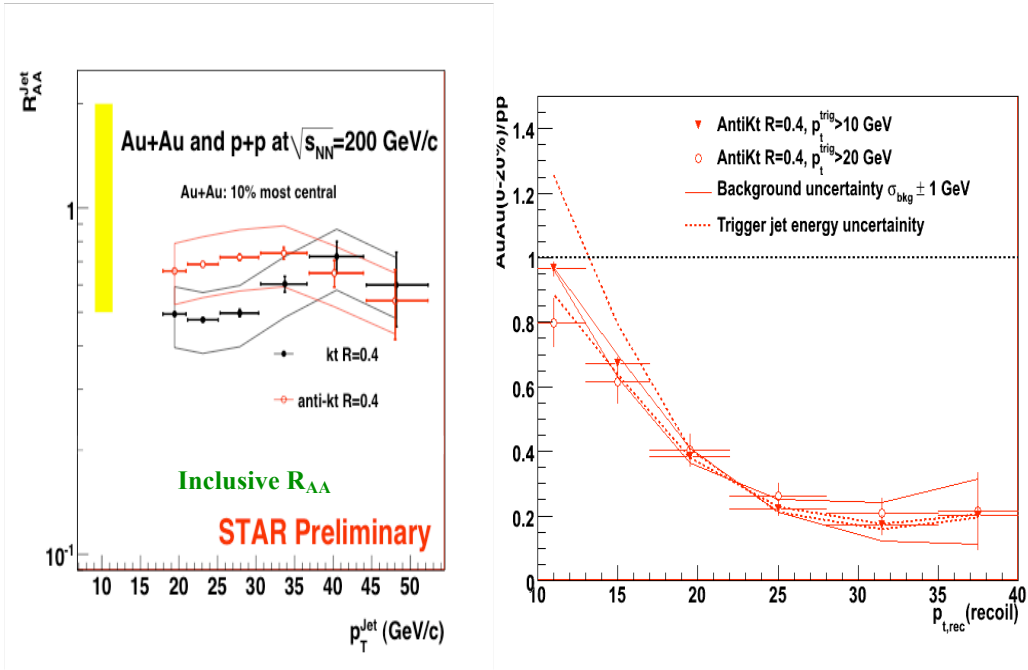
Figure 2.13: (Left) Jet R_{AA} for 10% central Au+Au collisions; (right) Ratio of di-jet coincidence rate for 20% central Au+Au collisions over p+p collisions at $\sqrt{s}$ = 200 GeV. From Ref. [13].

Combining both of these measurements suggests that partonic energy loss at RHIC manifests itself in a broadening of the jet structure, accompanied by an enhancement of low-z ($z=p_t^{hadron}/E_{Jet}$) particles in the jet fragmentation (See Figure 2.14 right).

Measurements of the jet fragmentation function and their modification, especially at high z, are currently limited to jet energies around 25-30 GeV and z<0.7 utilizing the recoil jet in the HT triggered Y07 data-set.
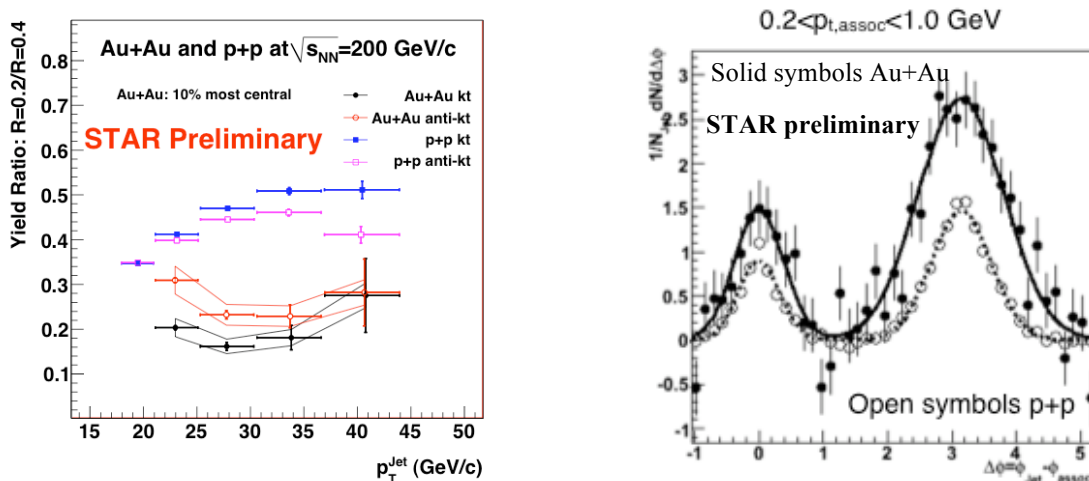
Figure 2.14: (left) Jet cross-section ratio R=0.2/R=0.4 for p+p collisions and 0-10% central Au+Au collisions; (right) Jet-Hadron correlations for HT triggered jets > 20 GeV and charged hadrons with 0.2<$p_{t,assoc}$<1 GeV/c. From Ref. [13].

The increase in the recorded statistics sampled by STAR in Y10 will open up the possibility to study the jet R_{AA} as function of centrality, thus testing the path-length dependence of partonic energy loss. The centrality dependence would also provide important systematics and possible new insights concerning background fluctuations in the underlying heavy-ion event and how elliptic flow affects the current background subtraction scheme. In addition the kinematic reach for the inclusive jet x-section, di-jet coincidence measurements and fragmentation functions will be extended beyond 40 GeV in jet energy. Furthermore, the full TOF acceptance in Y10 will allow the first PID (π, K, p) fragmentation function measurements and the study of the flavor dependence of jet-quenching.

2.5. Non-photonic Electron Measurements in STAR

Large heavy quark energy loss discovered through measuring high p_T non-photonic electron nuclear modification factor in 200 GeV central Au+Au collisions (R_{AA}) has triggered a lot of activities in the field trying to understanding the source. Although the R_{AA} measurements from STAR and PHENIX are consistent with each other, the measurements of high p_T non-photonic electron invariant yield in both p+p and Au+Au collisions differ by about a factor of two. Furthermore, there are also large differences in the total cross section measurements between the two experiments, indicating the discrepancy also appears in low p_T heavy flavor measurement. The dominant background for early STAR measurement was the large amount of conversion electrons originating from the silicon detectors, which leads to about 10 times smaller signal to background ratio than that of PHENIX. To resolve this discrepancy, starting from 2008 run, STAR decided to remove the silicon detectors to significantly reduce the photonic background. The comparison of the measurements between the low material run and early runs should tell us where the sources of the problem could be.

The first step we took is to focus on solving the problem in p+p collisions. We measure the non-photonic electron invariant cross section using the data from the low material 2008 p+p run as well as the high material 2005 run as a cross check.
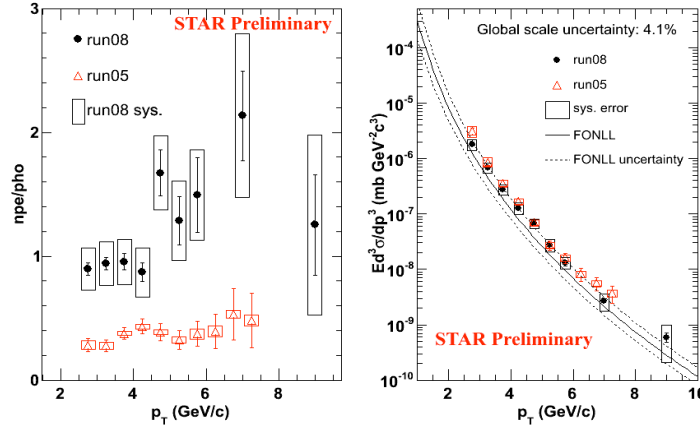
Figure 2.15: (left) ratio of non-photonic over photonic ratio in 200 GeV p+p collisions from 2008 (closed circles) and 2005 (open triangles) analysis. (right) invariant cross section of non-photonic electron production in 200 GeV p+p collisions from 2008 (closed circles) and 2005 (open triangles) analysis. From Ref. [14].

The left panel of figure 2.15 shows the ratio of non-photonic electron over photonic electron yield as a function of p_T obtained in 2008 (closed circles) and 2005 (open triangles) data analysis. The ratio in 2008 run is much higher due to the fact that there are much less material in front of TPC after removing the silicon detectors. The right panel of Figure 2.15 shows the non-photonic electron invariant cross section (($e^+ + e^-$)/2) as a function of p_T in $p + p$ collisions from the analysis of 2008 (closed circles) and 2005 (open triangles) run. Despite the large difference in photonic background, the two new measurements agree with each other very well.
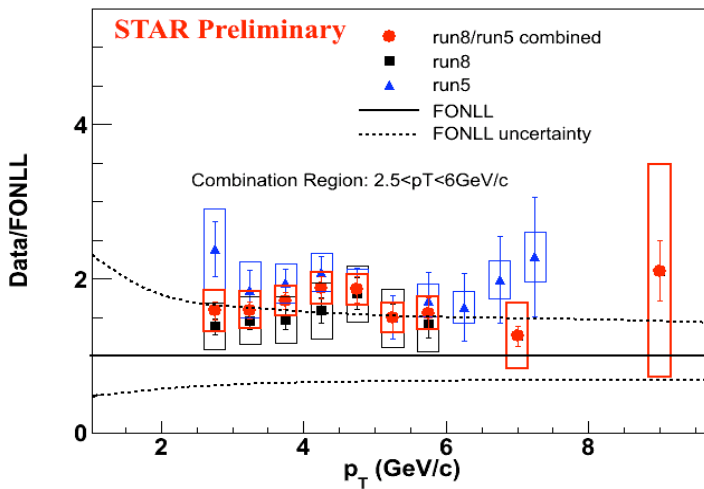
Figure 2.16: Ratio of invariant cross section measurement over FONLL using data from 2008 (closed black circles) and 2005 (closed triangles) runs. The red closed circles represent the result from combining 2008 and 2005 measurements. From Ref. [14].

To further clarify the agreement between the two measurements, we compare the ratio of each individual measurement over FONLL calculation as shown in figure 2.16, where the

closed triangles represent 2005 result, the closed black circles represent 2008 result and the red closed circles are the result of combining 2008 and 2005 measurement at p_T<6GeV/c through "Best Linear Unbiased Estimate" (BLUE) method. The BLUE method provides a $\chi 2$ test to check the consistency between two different measurements on the same physics quantities. The χ^2/ndf of our 2008 and 2005 measurements is 0.65, which means the two results are consistent with each other, Figure 2.17(a) shows the comparison of the new STAR invariant cross section measurement combining the new 2008 and 2005 results (closed circles) with the RHIC early published STAR result (closed triangles) obtained from 2003 run and PHENIX result (open triangles). Figure 2.17(b) shows the ratio of each individual measurement in (a) over the FONLL calculation. One can clearly see that STAR new measurement and PHENIX published result agree with each other within the quoted uncertainties.
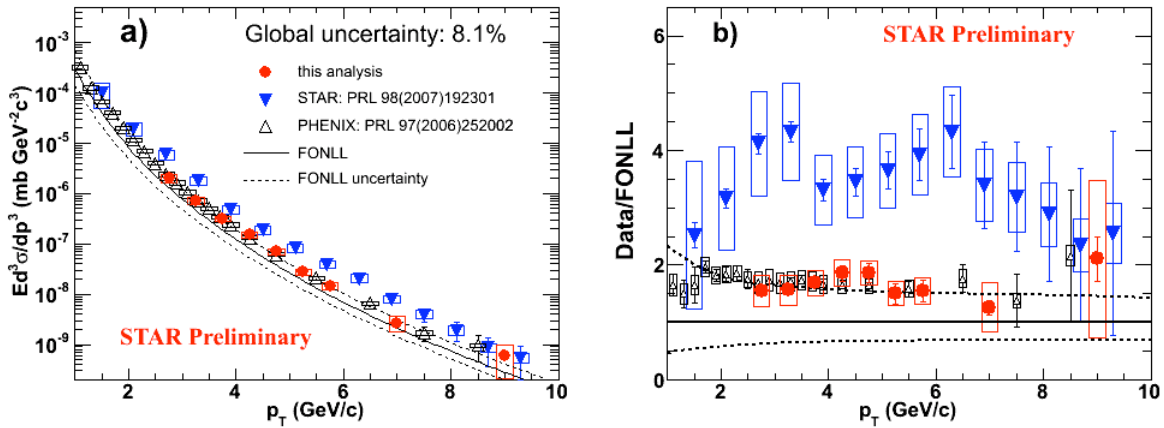
Figure 2.17: (a) Comparison of non-photonic electron invariant cross section from the new STAR measurements (closed circles) with the RHIC early published results, i.e. STAR (closed triangles) obtained from 2003 run and PHENIX (open triangles). The lines represent FONLL calculation and its uncertainty. (b) ratio of each individual measurement in (a) over the FONLL calculation. From Ref. [14].

The reasons for the difference between the new results from Runs 5/8 and the published STAR result from Run 3 [11,12] are under investigation. The dataset recorded at 200 GeV in Run 10 is the first run in STAR with both low material and ion-ion collisions. This provides us the opportunity to precisely address R_{AA}, by measuring differential NPE yields in Au+Au collisions under conditions and expected statistical accuracy similar to those from Run 8. STAR is also actively pursuing the analysis of low p_T NPE from the Run 8 and Run 9 datasets, along with low p_T muons and fully reconstructed D mesons from Run 9, in order to fully constrain the total cross section in p+p collisions and address inconsistencies between STAR and PHENIX. Similar analyses will be pursued in Au+Au collisions using the Run 10 dataset at 200 GeV, with the added advantage of full barrel TOF coverage.

References

[1] B. I. Abelev *et al.,* STAR Internal Note - SN0493, 2009.

[2] V. Koch *et al*., Phys. Rev. Lett. **95**, 182301(2005); M. Asakawa *et al*., Phys. Rev. Lett. **85**, 2072(2000).

[3] B. Berdnikov *et al*., Phys. Rev. **D61**, 105017(2000).

[4] M. A. Stephanov, Phys. Rev. Lett. **102**, 032301(2009); K. Rajagopal and M. A. Stephanov, private comm. 2009.

[5] M. Asakawa *et al.,* Phys. Rev. Lett. **103**, 262301(2009).

[6] M. Cheng *et al.,* Phys. Rev. **D79**, 074505(2009); B. Stokic *et al.,* Phys. Lett. **B673**, 192(2009).

[7] Y. Hatta *et al*., Phys. Rev. Lett. **91**, 102003(2003).

[8] M. M. Aggarwal *et al.,* arXiv: 1004.4959.

[9] B. I. Abelev *et al*., (STAR Collaboration), arXiv: 1004.4959.

[10] J. Adams *et al.,* (STAR Collaboration), Nucl. Phys. **A757**, 102(2005).

[11] B. I. Abelev *et al*., (STAR Collaboration), Phys. Rev. Lett. **98**, 192301(2007).

[12] Z. Xu for STAR Collaboration, SQM2008 Proceedings.

[13] M. Ploskon for STAR Collaboration, Nucl. Phys. **A830**, 255c(2009).

[14] W. Xie for STAR Collaboration, DIS2010 Conference, 2010.

3. Study of the QCD Phase Diagram and Properties of QGP

3.1. Completion of Phase-I of Beam Energy Scan Program in Run 11

The critical point search part of the BES program requires a careful choice of stepping in μ_B for this experimental driven approach to locate CP. A non-monotonic dependence of observables sensitive to CP on $\sqrt{s_{NN}}$ and an increase of long-wavelength fluctuations should become apparent only near the critical point. The rise and then fall of this signal as μ_B increases should allow us to ascertain the (T, μ_B) coordinates of the critical point. Note that the magnitude of these non-monotonic excursions, as well as the probability that they will survive the final state interactions, is difficult to predict. Fortunately for the experiments, there may not be a need for the systems evolution trajectory to "pass" precisely through the critical point in the (T, μ_B) plane to see the signatures, as some hydrodynamic calculations show that the critical point "attracts" trajectories [1]. In such a case, if the trajectory misses the critical point by a few tens of MeV along the μ_B axis, the signature will be just as strong as if it were to pass directly through it. Note, however, that this "attraction" is not generic, and relies on specific features of the EOS near the critical point [1]. Available lattice QCD calculations suggest the μ_B region of influence around CP would be around 100 MeV [2].

Although subsequent phases of BES running can use smaller steps in μ_B to verify and trace the possible effect of focusing and to pin down the critical point, the first exploration phase was proposed to step in μ_B such that with a few steps in $\sqrt{s_{NN}}$ we may narrow down to an area of interest for further study (see Table 3.1 for the beam energies and corresponding μ_B values [3]). Thus 18 and 27 GeV collisions crucially bridge the gap in μ_B corresponding to about 200 MeV between 39 and 11.5 GeV collisions for which STAR took data in Run 10.

Beam Energy (GeV)	Baryon Chemical Potential, μ_B (MeV)
5.0	550
7.7	410
11.5	300
18	230
27	151
39	112

Table 3.1: Beam energies and corresponding expected baryon chemical potentials.

The following is our proposal for completion of Phase-I of the BES program in Run 11. It is consistent with the BUR for Run 10 and with the PAC recommendation, but has been updated to reflect information from Run 10. Both event rates and data taking efficiency were higher than expected in Run 10, with an average of approximately 85 hours/week of data taking at energies above injection and 100 hours/week at energies for which no ramping is necessary. We give a revised estimate of days required for each remaining BES energy point to meet STAR physics goals in Table 3.2. In Run 10, we have completed our

goals at 39 GeV, 11.5 GeV, 7.7 GeV, and beam tests at 5 GeV. The remaining beam energies are 18 GeV and 27 GeV. In addition, we support any additional work C-AD wants to do at 5 GeV in Run 11.

Beam Energy (GeV)	Event Rate (Hz)	Run10 BUR request	Run 11 request	Revised estimate based on Run 10 performance
18	200	15 M	100 M	1 week
27	400	33 M	150 M	1 week

Table 3.2: BUR for 18 and 27 GeV Au+Au collisions to complete the Phase-I BES program.

From the excellent RHIC performance in Run 10, we project that we could complete our previously stated goals at 18 and 27 GeV in a few days at each beam energy. We do believe that in order to effectively use the collider to run an energy setup, it is much better to increase the request for the length of time at each energy to one week, the shortest amount of time we believe reasonable. The one-week run will also enhance our physics program significantly. We project that running for this amount of time will lead to much richer data samples, including measurements of hypertriton production at the 7-8 sigma level and significant signals such as the ϕ and ω in the di-lepton channel.

3.2. Physics of 200 GeV U+U Collisions at RHIC

3.2.1. Introduction

The commissioning of the EBIS upgrade will enable Uranium beams to be accelerated at RHIC. The larger A value and the prolate shape of Uranium opens up a new horizon of measurements at RHIC, in which we can generate matter with higher densities than in Au+Au collisions and study the path-length dependence of jet-quenching.

Grazing (non-central) collisions of spherical nuclei produce elliptic shaped overlap areas. The interactions in and expansion of the spatially asymmetric fireball lead to large asymmetries in momentum space. Since the spatial asymmetry quickly washes out, the observed momentum space asymmetries are a sensitive probe of the early dynamics of the expanding system. These anisotropies are quantified by the various coefficients in the Fourier expansion of the azimuthal distribution of the transverse momenta (or number of particles). The second coefficient, v_2, is a measure of anisotropy arising due to the elliptic shaped overlap zone. For low densities, v_2 should depend on both the initial state spatial anisotropy (eccentricity ε) and the scattering length. With sufficient rescattering in high enough densities in the transverse plane, the matter in the produced fireball may reach thermalization. The hydrodynamic limit assumes complete thermalization, with a mean free path much smaller than the system size, where the values of v_2 may depend only on the initial state spatial anisotropy so that v_2 is proportional to ε. While results on v_2 scaled with the initial state spatial anisotropy ε for smaller colliding systems at lower center of mass energies have shown a linear dependence on the transverse particle density, as expected from the low density approximation, v_2/ε for nearly central Au+Au collisions at 200 GeV approaches values close to those predicted for a system with zero mean-free-path where a

hydrodynamic description of the expansion becomes applicable. Ideally, one would like to investigate the effect of an increase in transverse particle densities on values of v_2/ε, to probe well into the region of hydrodynamic scaling to confirm the relevance of a hydro limit. While saturation of scaled anisotropy with increasing transverse particle densities would validate the existing hydro models, a linear increase in its value would imply a different value of the hydro limit arising from a stiffer equation of state.
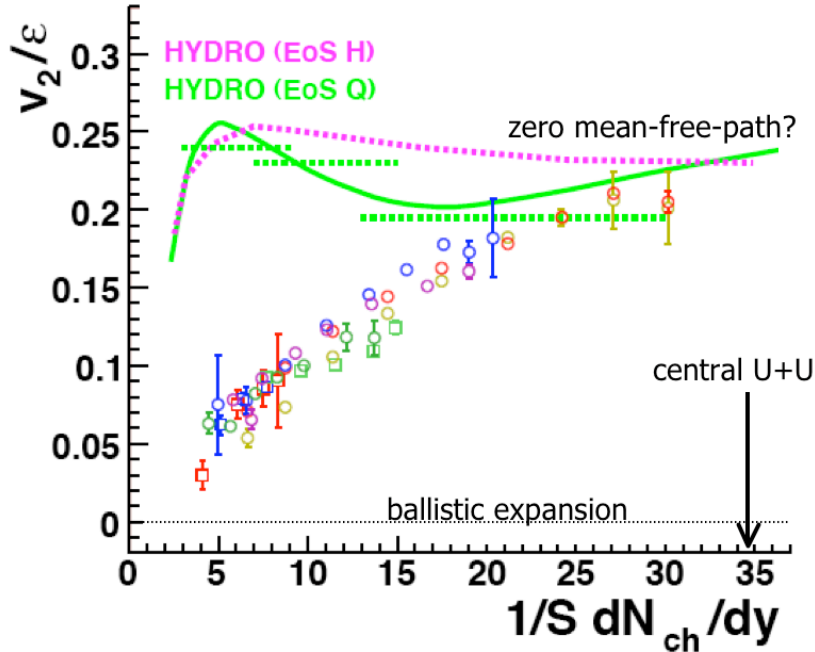

Figure 3.1: Heavy ion data on eccentricity scaled v_2 vs. transverse particle density. A central U+U collision is expected to reach densities 30% larger than central Au+Au while the eccentricity is large. Estimates for $1/S\ dN_{ch}/dy$ from [4].

The Pb ion beams at the Large Hadron Collider at CERN will provide an opportunity to probe the hydro limit by increasing the transverse particle densities by approximately a factor of 2 above those at RHIC. U+U collisions can bring experiments at RHIC a significant fraction towards this increase, with estimates ranging from a 30% to 50% increase in entropy and energy density in central U+U collisions as compared to central Au+Au collisions [4-8]. Because Uranium is highly deformed with $\beta=0.28$, the maximum energy density can be reached in the most central tip-tip collisions (head-on collisions with both long axes aligned) while the largest ε will be generated in body-body collisions (head-on collision along both short axes). Recently, Monte Carlo Glauber simulations have shown [9] that compared to the spherical Au+Au collisions, the anisotropy parameter v_2 is enhanced more than 10% in most central U+U body-body collisions. On the other hand, the nuclear modification factor R_{AA} is further suppressed to 0.1 in tip-tip U+U central collisions as compared to 0.2 in most central Au+Au collisions.

One major advantage of accelerating Uranium nuclei, as compared to any more spherical nuclei, is the possibility of a large initial-state spatial anisotropy in central collisions, depending upon the relative orientation of the two nuclei at the time of collision. The large

particle densities in central collisions, along with the large values of the eccentricity, will provide a unique opportunity to probe the hydro limit at available RHIC energies.
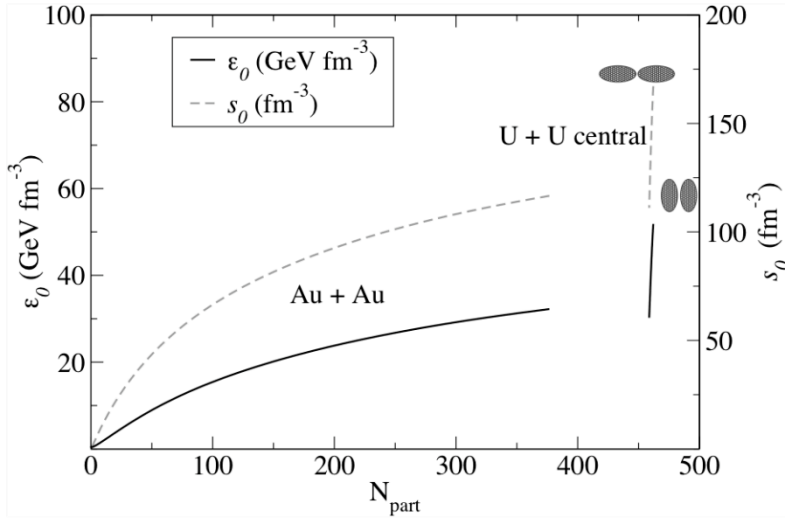

Figure 3.2: Schematic of achievable energy density (ε_0) and entropy density (s_0) in U+U collisions, for two extreme geometrical cases. Figure from [7].

It is imperative that one estimates the effect of the non-spherical shape of Uranium nuclei on the various parameters that help probe the hydro limit. Model calculations using an initial state geometry based on a Glauber model and using a two component model for obtaining the charged particle multiplicities are used to estimate the multiplicities expected in Uranium+Uranium collisions in different orientations. The free parameters of the two component models have been fixed using Au+Au data at RHIC energies. The multiplicities for different centralities and different orientations have also been estimated using the KLN model, incorporating saturation physics through the Color Glass Condensate. Both models can reproduce existing multiplicity data in Au+Au collisions. The two different models differ however, in their predictions for the shape and width of the multiplicity distribution in fully central U+U collisions (see Figure 3.3). These differences provide a clean test to distinguish between the phenomenological two-component model and the CGC based model. While the two-component model yields a broader double hump multiplicity distribution, the CGC based model gives a narrower distribution. The double hump structure in the two-component model arises because while both tip-tip and side-side collisions have the same number of participants, the tip-tip collisions yield a larger number of binary nucleon-nucleon collisions. For that reason, high multiplicity central events are dominated by tip-tip collisions. The fKLN-CGC model with a constant p_t cut at 3 GeV in the k_t factorization formula actually produces more multiplicity in the body-body collisions than the tip-tip collisions: this is opposite to the two-component model. Removing that cut yields a distribution closer to the two-component model but still narrower. It's clear therefore that the multiplicity distribution in central U+U collisions is a sensitive probe of how entropy is produced in nucleus-nucleus collisions. In addition to the width of the distribution, it will be possible to measure v_2 as a function of the multiplicity in central U+U collisions to ascertain how correlated high multiplicity events are with large eccentricity. Figure 3.5 shows the variation of eccentricity with multiplicity in the top 1% most central U+U collisions. These data will provide an independent check of the CGC based

multiplicity model in a regime where saturation effects should be strong and the formalism should be most valid.

Once a multiplicity model has been validated for U+U collisions, one can make use of that model to select event samples with varying eccentricities as shown in Figures 3.3 and 3.4. The distributions of eccentricities for the class of events obtained using the above mentioned models are shown in Figure 3.4.
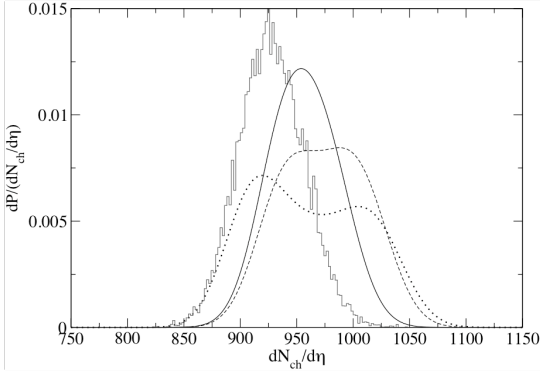
Figure 3.3: $dN_{ch}/d\eta$ for full-overlap U+U collisions. Dotted curve from Glauber + two-component model, dashed and solid curves from CGC-related KLN model with two p_T cuts, histogram from cutting on the 0.5% fraction with lowest number of spectators. Figure from [8].
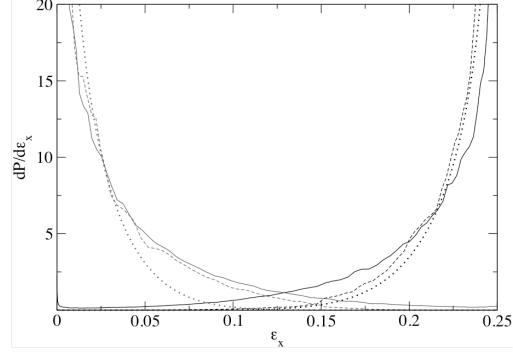
Figure 3.4: Eccentricity distribution for full-overlap U+U collisions, obtained by cutting the multiplicity distribution in Figure 3.3 on the 10% lowest or highest multiplicities. Dotted curve from Glauber + two-component model, dashed and solid curves from CGC-related KLN model with two p_T cuts. Figure from [8].

Despite quantitative differences between results of model calculations, in Figure 3.4 the qualitative features of U+U collisions remain: there are broad classes of central U+U events, either tip-on-tip with likely large multiplicity and small eccentricity or side-on-side with likely small multiplicity and large eccentricity, which can be selected with distinct experimental signatures. Other selection criteria, such as directly selecting on the strength of v_2 event-by-event [6] or selecting asymmetries in rapidity, are under active investigation.

Beyond investigating geometry and hydrodynamic behavior, the grossly deformed overlap zone will enable investigations in several other important areas; the path-length dependence of energy loss (dE/dx(L)), Local Parity Violation (LPV) and Ultra-Peripheral Collisions (UPC)

dE/dx(L): Current theories of energy loss for fast partons assume a non-linear dependence on path-length, but this has not yet been tested in experiment, partially because of the small difference in path lengths for the parton traversing in plane and out of plane. Side by side U+U collisions are expected to provide almost twice as much difference between the in plane and out of plane path lengths for the same eccentricity as semi-peripheral Au+Au collisions. With modest data samples, these path length effects can be investigated via

single-hadron and di-hadron suppression, as done in RHIC Runs 1,2, and 4. More detailed investigations utilizing rarer probes await high luminosity running.

LPV: Parity is conserved in the strong interaction, but local parity violation has long been expected because of the topological structure of QCD. A signal of local parity violation, from the chiral magnetic effect [10] and the strong QED magnetic field in non-central collisions, may have been observed in high-energy nuclear collisions [11]. Since the observable used is parity even, there is a possibility that more mundane processes can mimic the signal of local parity violation. The magnetic field required for the parity-violating signal can only exist in non-central collisions, as it is produced mainly by the spectators as they travel from the collision zone. In fully central U+U body-body collisions, there are no spectators, while in certain configurations the geometry of the collision zone induces v_2. The signal from true local parity violation should therefore be small, while possible backgrounds should remain strong. One therefore can use the 'central U+U body-body' collisions, where the field should be small or zero, to further test if the observations in Ref. [11] originate from local parity violation or more mundane background processes.

UPC: The unique geometry of U+U collisions also opens up an exciting possibility in Ultra-Peripheral Collisions studies. These studies are based in coherent phenomena across the entire nucleus, which can be affected significantly by quantum correlations. The geometry of U+U collisions can enhance the probability for multiple vector meson production and multi-photon interactions to occur. Based on the production rates for single and double ρ production [12] and assuming the cross-section scales as $Z^8*[A^{5/3}]^2$, about 1 out of 1,000 ρ^0 should be accompanied by a second ρ^0. Such multi-ρ samples enable the study of quantum correlations in production and decay, in which stimulated decay is a possibility.

3.3. Run 11 U+U at 200 GeV Request

The physics of U+U collisions can be split into two distinct classes, which have distinct requirements for beam conditions. The first class consists of bulk observables, such as multiplicity, elliptic flow, HBT, and the like. These have relatively small requirements in terms of the number of events, and are mainly focused on hydrodynamic behavior of the medium, though some measurements related to hadron quenching in medium can be made with such samples (as in the first years of RHIC Au+Au). This class also contains the light vector meson portion of the Ultra-Peripheral Collision program.

The second class of measurements consists of rare, triggered probes, such as γ-hadron, jets, and heavy flavor suppression, which are extremely luminosity hungry. Due to the large configuration space for the relative orientation of the two U nuclei at the collision point, restrictive cuts on data samples need to be made in order to select the most interesting densities and geometries. The authors of [7] and [8] advocate placing 0.5% cuts on spectators, combined with 5-10% cuts on multiplicity, decreasing sample sizes from minimum bias by a factor of a few thousand. This implies that rare probes need high luminosities, which are likely not achievable in Run 11.

With DAQ1000 and a modest collision rate of 5-10 kHz, we estimate that STAR can accumulate 400M events, approximately half central and half minimum bias, in 4 weeks'

time. The central trigger will likely be based on the number of spectator neutrons seen in the ZDC, which has single-neutron resolution and has been used successfully in all previous Au runs as a centrality trigger. The precise selection of centrality fraction in this trigger will depend on available collision rates.

Such a sample should allow for sufficiently fine-grained selection of geometries to investigate the behavior of v_2, HBT with respect to the reaction plane, and related measurements. It will also allow for some measurements related to jet quenching, such as suppression of single-hadron spectra and di-hadron correlations, at accuracies approximately at the level investigated in Au+Au collisions in Runs 2 and 4.
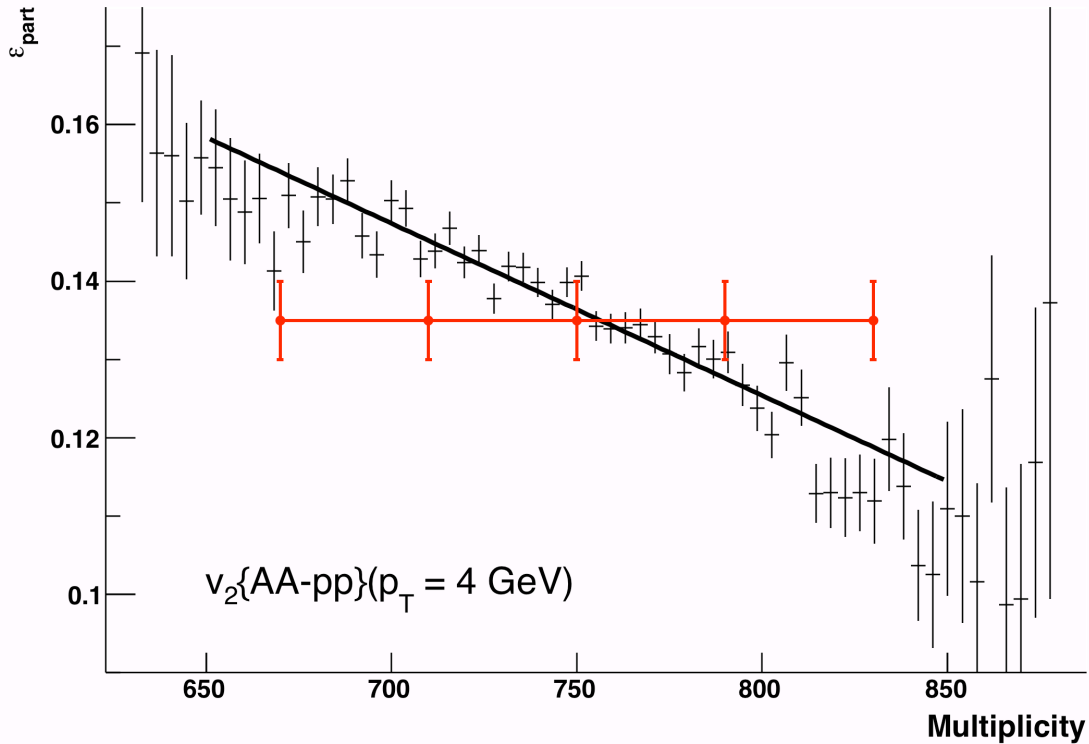
Figure 3.5: Black: $\langle \varepsilon_{part} \rangle$ as a function of measured mid-rapidity multiplicity in the most 1% central U+U collisions, as selected by the number of participants. Red: estimated uncertainties on $v_2\{AA\text{-}pp\}$ for p_T=4 GeV/c for such events, as selected with the ZDCs.

Examples of statistical uncertainties for two processes of interest are shown in Figure 3.5 and 3.6. Fig 3.5 shows the projected v_2 at p_T of 4 GeV/c, as a function of multiplicity in the 1% most central collisions as determined by the spectator neutrons in the ZDCs. With 200M 0-10% central ZDC events, each multiplicity bin contains approximately 2M events, and so has equivalent statistics to the Run 2 central data set. Also shown on the figure is a calculation of the expected change in v_2 over this range in multiplicity, as estimated from the participant eccentricity ε_{part} as calculated in a Monte Carlo Glauber model. Figure 3.6 shows the projected accuracy of R_{AA} for $p_T > 6$ GeV/c, again as a function of multiplicity for the 1% most central collisions as selected by the ZDCs, along with the possible range

over which R_{AA} may be expected to vary. In both cases, statistical accuracies are sufficient to assess the level to which the cuts select on the geometry of the collision, rather than on fluctuations.
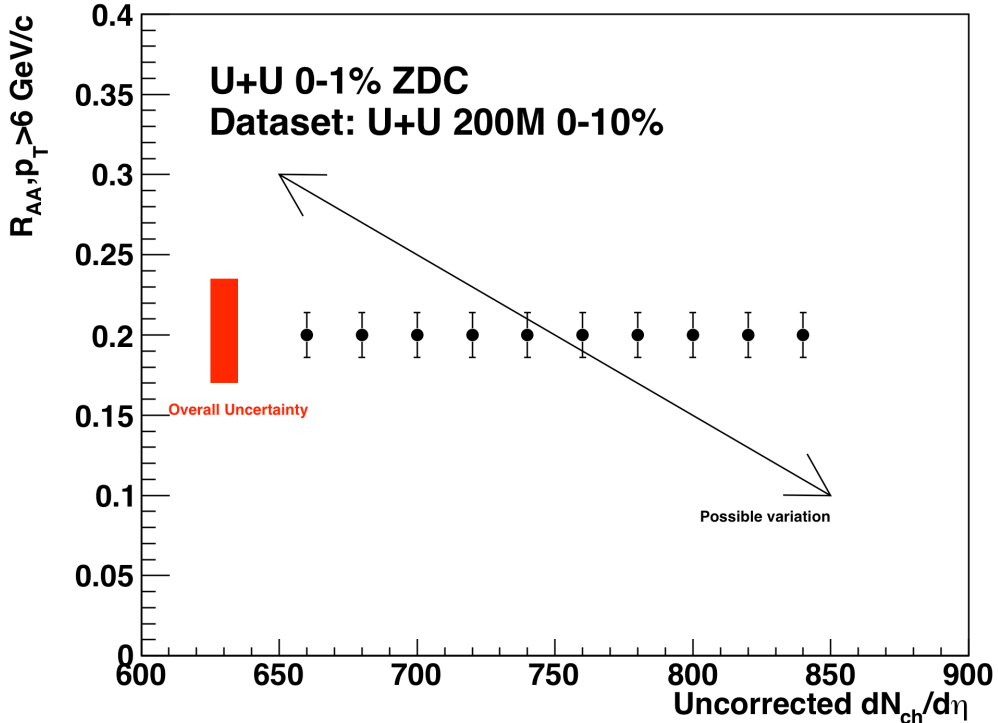
Figure 3.6: Projected R_{AA} as a function of measured mid-rapidity multiplicity for the 1% most central collisions, as selected with the ZDCs. Red box shows overall uncertainty, common to all points, while error bars show point-to-point uncertainty, dominated by statistical uncertainty. Arrow shows possible range of variation across this multiplicity range.

The main purpose of the U+U run in Run 11 is to better understand entropy production and possible saturation effects in A+A collisions and to establish the level to which unique geometric configurations can be selected beyond fluctuations. We need a sufficient dataset to see statistically significant variation in physical quantities, such as R_{AA} and v_2, in order to find the point at which fluctuations dominate over physical variations. At somewhat coarser granularity in geometrical selection, signals of local parity violation can be studied. We estimate that such a dataset will take 4 weeks to obtain. For this first run, slightly lower energy beams are acceptable, as may be necessary with the lower Z/A of U vs. Au, but for precision high luminosity tests in the future it would be preferable to match energies with other collision systems.

3.4. Run 12 High Luminosity Heavy Ion Collisions

With the improvements in stochastic cooling, Run 12 provides an opportunity to dramatically increase sampled luminosity on the way to RHIC II. Both U+U and Au+Au collisions are expected to have essentially equivalent parton-parton luminosities for hard

processes, or A^2*L. This would mean approximately 2/3 the integrated luminosity for U+U vs. Au+Au. In a 10-week run, we expect to be able to sample 5 nb^{-1} of Au+Au collisions, which is equivalent to 200 pb^{-1} of p+p collisions, and is approximately twice the total sampled in Run 10. Table 3.3 shows the current highest sampled luminosities with the full component of detectors for various species at 200 GeV, along with their equivalent luminosities.

| Run and species	Integrated Luminosity	Equivalent p+p luminosity A*B*L [pb^{-1}]
Run 8, d+Au 200 GeV	34 nb^{-1}	13
Run 9, p+p 200 GeV	23 pb^{-1}	23
Run 10, Au+Au 200 GeV	2.6 nb^{-1}	100
Run 12, Au+Au (U+U) 200 GeV	5 nb^{-1}	200

Table 3.3: Maximum sampled luminosities by species and run, at 200 GeV. Run 12 is also projected.

The decision as to whether to run U+U or Au+Au in Run 12 awaits results from Run 11. While the equivalent luminosities are expected to be similar, each species has advantages and disadvantages. The U+U collisiosn has the advantage of higher maximum entropy density, and therefore potentially stronger medium effects, along with the capability to explore the effect of different geometrical configurations at the high density of central collisions. This advantage is also its disadvantage, as it can lead to fluctuations in conditions for luminosity-hungry analyses that cannot afford the statistical hit of fine bins in centrality. The extent to which these fluctuations matter awaits the first look in Run 11.

Run 12 is also only a step towards the full luminosity of RHIC II. This step is important for analyses that depend on electrons, since shortly after Run 12 the inner configuration of the STAR detector, currently free of material except the beam-pipe and air, will be upgraded with components of the Heavy Flavor Tracker. This upgrade enables high precision identification of open heavy flavor, but has irreducibly deleterious effects on the identification of quarkonia using electrons, due to increased Bremsstrahlung. The installation of the Muon Telescope Detector by 2014 will enable precision measurements of quarkonia in the muon channel.

As an example of the physics reach of high luminosity, Figure 3.7 shows projected uncertainties for one bin in $z_T = p_T^{associated}/E_T^\gamma$, using the techniques of a recent STAR publication[13]. This bin, at low z_T but high E_T^γ has maximal distinguishing power between models, as shown in the figure. All models shown reproduce the suppression pattern for hadrons, but differ in their treatment of the geometry of the collision zone and the detailed distribution of energy loss by the parton. While these models are indistinguishable at current statistical power, the increased statistical power of the high luminosity datasets will enable the models to be distinguished. Since the parameters of the medium deduced from these models differ by a wide range, excluding some models will

enable a more precise understanding of the properties of the medium created in heavy ion collisions at RHIC, and in the mechanism of energy loss.
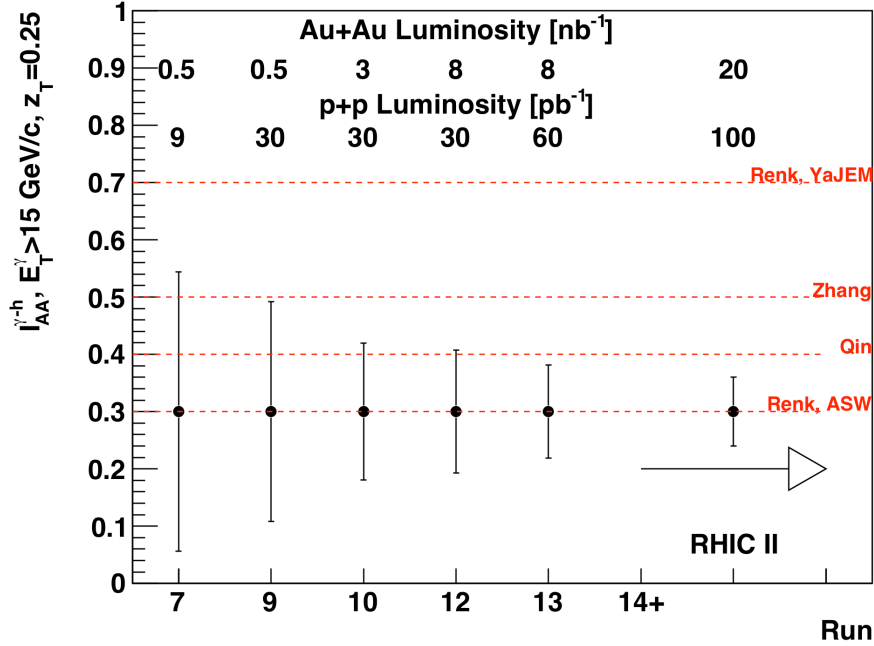

Figure 3.7: Projection of statistical uncertainties in the ratio between central Au+Au and p+p of away-side yield of hadrons associated with a trigger direct photon, $I_{AA}^{\gamma-h}$, as a function of RHIC Run and increasing cumulative luminosity sampled. The lines show predictions for this ratio. (Renk, YaJEM and Renk, ASW[14], Zhang[15], Qin[16])

Another suppression measurement requiring high luminosity is the suppression pattern of the Upsilon states. The production of Upsilon 1S is not expected to be suppressed for the energy densities reached at RHIC, while the 2S and 3S are expected to show some suppression. Unlike the J/Psi at RHIC or Upsilon production at the LHC, coalescence of beauty quarks in the late stage of medium evolution is not expected to be a significant component of Upsilon production at RHIC, so the pattern of suppression of the states provides a relatively clean probe of the energy density of the medium. Results from RHIC Run 6 [17] and Run 7 from STAR and PHENIX have produced only upper limits for the suppression of the sum of the three states. Higher luminosity is sorely needed for these clean measurements.

Figure 3.8. shows a preliminary lineshape from Run 9 p+p collisions at √s=200 GeV, from a first pass through an integrated sample of approximately 20 pb⁻¹, and with the current low material budget in STAR. A clear signal is seen above like sign background, with high significance. Drell-Yan and correlated semileptonic beauty decays produce a broad continuum on which the Upsilon states sit, which for this data is cut off by triggering below approximately 8 GeV in mass.
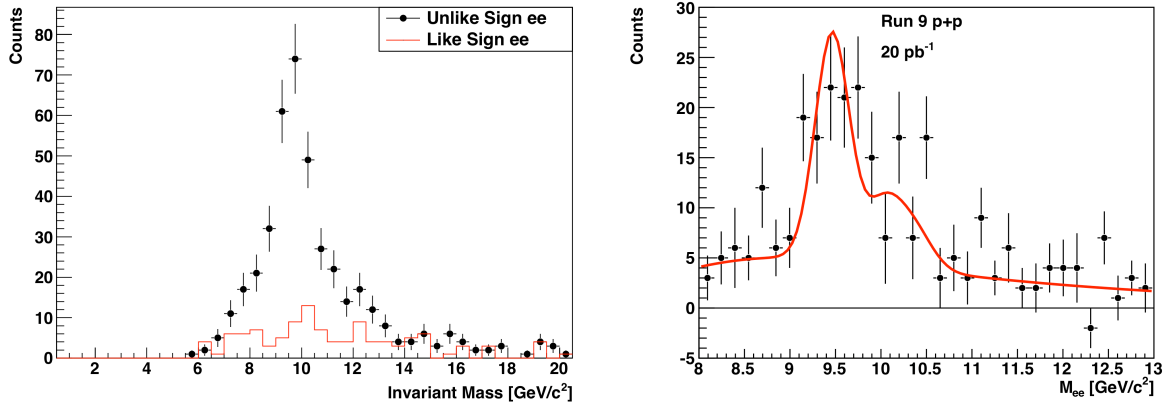
Figure 3.8: Invariant mass distribution around the Upsilon mass, from p+p Run 9 at √s=200 GeV. Triggering affects the invariant mass distribution below approximately 8 GeV. Right: Like-sign subtracted e$^+$ e$^-$ invariant mass distribution at finer mass scale, along with parameterization of the line shape with the three Upsilon states, trigger inefficiency, and continuum background.
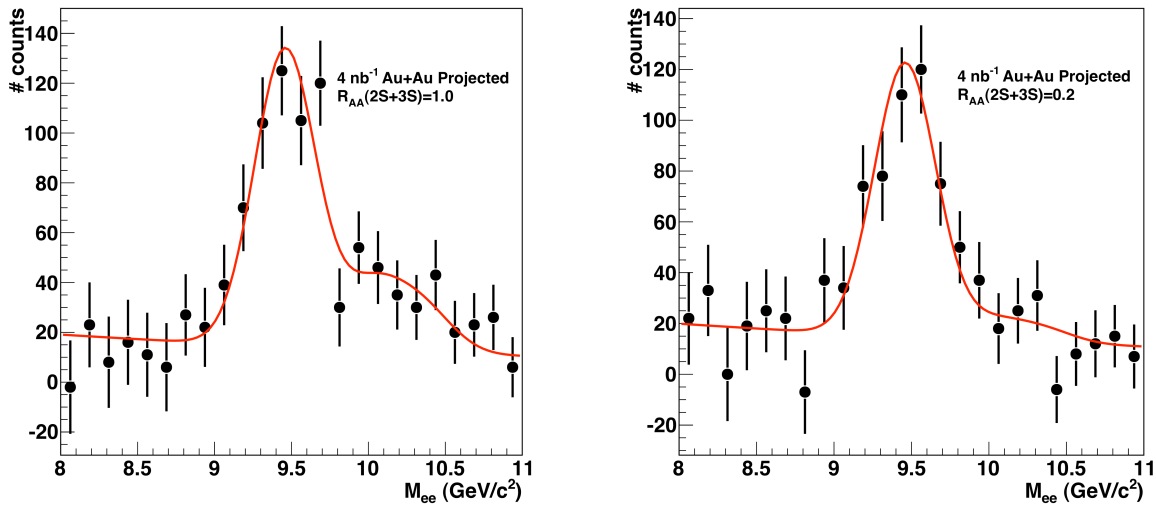
Figure 3.9: Projected invariant mass distributions for the combined dataset from Run 10 and Run 12. In the left panel, R$_{AA}$ for the Upsilon 2S and 3S is assumed to be 1, while in the right panel it is assumed to be 0.2.

Equivalent luminosity for the combined dataset of Au+Au Runs 10 and 12 is projected to somewhat less than an order of magnitude above that in Figure 3.8, assuming that R$_{AA}$ = 1. Figure 3.9 shows a projection of the invariant mass distribution as it would be from this combined measurement, in which the integrated luminosity is assumed to be approximately half that of the full dataset due to the need to restrict the vertex to minimize material at high vertex z. Combined with later increases in the p+p reference luminosity, quantification of R$_{AA}$ of the Upsilon 1S at the 10-20% level should be possible, along with a first measurement of the R$_{AA}$ of the Upsilon 2S+3S. Further precision awaits the installation of the Muon Telescope Detector to move to the dimuon channel, which in most high energy

experiments is the channel of choice for the separation of Upsilon states, due to the absence of Bremsstrahlung tails.

Fully reconstructed jets can also benefit greatly from Run 12. Figures 2.13 and 2.14 show results from approximately 7M central events in Run 7 [18]. In Run 10, STAR collected 250M central events, or an increase in statistical power over Run 7 by a factor of 35. This data sample contains all central events, regardless of its momentum structure, and so is useful for an unbiased set of jets. Another data sample from Run 10, the high tower trigger sample, selects a highly biased set of jets, which can be used in some ways for dijet studies but not for fully inclusive measurements. The biases introduced by high tower triggers are tightly coupled to the jet modifications that are of interest, a coupling that cannot be overcome for many measurements of interest. This sample corresponds to another factor of 6 higher central events, or 1500M. For Run 12, work is ongoing to increase trigger capability to select a less biased set of jets than is currently available with a high tower trigger. Should this be successful, a sample corresponding to 3000M central events would be available for unbiased studies, reflecting an increase by a factor of 400 in statistical power over the reach shown in figure 2.13 and 2.14.

References

[1] M. Asakawa *et al.,* Phys. Rev. Lett. **101**, 122302 (2008).
[2] R. V. Gavai and S. Gupta, Phys. Rev. **D78**, 114503 (2008).
[3] J. Cleymans, H. Oeschler, K. Redlich, and S. Wheaton, Phys. Rev. **C73**, 034905 (2006),
[4] C. Nepali *et al*., Phys. Rev. **C73**, 034911(2006).
[5] A.J. Kuhlman and U.W. Heinz, Phys. Rev. **C72**, 037901(2005).
[6] C. Nepali *et al.,* Phys. Rev. **C76**, 051902(R)(2007).
[7] U.W. Heinz and A.J. Kuhlman, Phys. Rev. Lett. **94** 132301(2005).
[8] A.J. Kuhlman, U.W. Heinz, and Y. Kovchegov, Phys. Lett. **B638**, 171(2006).
[9] H. Masui, B. Mohanty and N. Xu, Phys. Lett. **B679**, 440(2009).
[10] D. Kharzeev, R. D. Pisarski and M. H. G. Tytgat, Phys. Rev. Lett. **81**, 512(1998) and references therein.
[11] B.I. Abelev, *et al.,* (STAR Collaboration), Phys. Rev. Lett. **103**, 251601(2009); *ibid,* Phys. Rev. C, in Print, 2010; arXiv: 0909.1717 [nucl-ex].
[12] S. Klein and J. Nystrand, Phys. Rev. **C60**, 014903(1999).
[13] B.I. Abelev *et al.,* (STAR Collaboration), arXiv:0912.1871.
[14] T. Renk, Phys. Rev. **C80**, 014901(2009).
[15] H. Zhang *et al.,* Nucl. Phys. **A830**, 443c(2009).
[16] G.-Y. Qin *et al*., Phys. Rev. **C80**, 054909(2009).
[17] B.I. Abelev *et al.,* (STAR Collaboration), arXiv:1001.2745.
[18] M. Ploskon *et al.,* (STAR Collaboration), Nucl.Phys. **A830**, 255c(2009).

4.   Study of Polarized p+p Collisions

4.1.   Introduction

The STAR spin physics program studies proton spin structure in terms of quarks and gluons, and the dynamics that underlie transverse spin phenomena observed in proton collisions at forward pseudo-rapidities. This program is complemented by polarized elastic scattering measurements with Roman Pots, which enable also the study of central particle production in scattering that leaves the beam protons intact (e.g. double-Pomeron exchange).

To advance the STAR spin physics program we request 10 weeks of polarized proton-proton operations at $\sqrt{s}$ = 500 GeV in Run 11. The 10 weeks would serve continued commissioning and development of RHIC luminosity, polarization, and polarization measurement. We would use four weeks, or a delivered integrated luminosity of about 40pb^{-1}, for spin physics measurements with transverse beam polarizations and the remainder, amounting to about a delivered 125 pb^{-1}, for spin measurements with longitudinal polarizations. Average beam polarization values in store are anticipated to be in the range of 35% to 50%. The period with transverse polarization directions should allow first measurements of transverse single spin asymmetries A_N for inclusive probes in the region of the Forward Meson Spectrometer at $\sqrt{s}$ = 500 GeV collision energy, as well as initial correlation studies. The period with longitudinal polarization directions should allow significant improvement of the mid-rapidity measurement of the asymmetry A_L for W^+ and W^- production and subsequent leptonic decay. If delivered beam polarizations are at the high end or exceed the anticipated range, a meaningful start would be made to measure gluon polarization at $\sqrt{s}$ = 500 GeV. In addition, we request 1 week of large ß* polarized proton-proton operations with transverse polarizations at $\sqrt{s}$ = 500 GeV in Run 11 for elastic scattering and central production measurements with the existing Roman Pot setup.

The integrated luminosities in our request are based on the RHIC Collider Projections (FY 2011 - FY 2015) document of May 11, 2010. We assume a mid-point of the projected minimum and maximum delivered integrated luminosities, and scale by 60% to account for the anticipated STAR data sampling efficiency. We consider it essential for the success of the $\sqrt{s}$ = 500 GeV longitudinal spin physics program to measure (anti-)quark polarizations and gluon polarization that proton beam polarizations of 50% or more, at the high end of or exceeding the RHIC Collider Projections, are achieved routinely and reproducibly during physics production running towards the end of Run 11. With this assumption, and with the provision that the STAR Forward Gem Tracker upgrade continues to proceed as planned and will be ready for physics by Run 12, we request 10 weeks of proton-proton physics production operations at $\sqrt{s}$ = 500 GeV with longitudinal polarizations in Run 12. This will allow first measurements of charge-separated longitudinal single-spin asymmetry measurements for W^+ and W^- production at forward rapidity via the decay channel into positrons and electrons. Precision in this measurement and in measurements of $\Delta g(x)$ at $\sqrt{s}$ = 500 GeV can be achieved with 300 pb^{-1} sampled luminosity and 70% beam polarization, and forms a multi-year goal.

4.2. RHIC Performance in Run 9

RHIC has, for the first time, brought in collision polarized proton beams at a center-of-mass energy of $\sqrt{s}$ = 500 GeV at the STAR IP during Run 9. Significant experience was gained with the acceleration and collisions of proton beams for both transverse and longitudinal polarization directions at this energy. The initial STAR goals at $\sqrt{s}$ = 500 GeV for Run 9 (c.f. section 4.3) were reached and RHIC Collider Projections for future beam periods can now be benchmarked.

The physics production period at $\sqrt{s}$ = 200 GeV in Run 9 has resulted in a sampled integrated luminosity of ~25 pb^{-1} with ~54% average longitudinal beam polarizations, well below the 50 pb^{-1} integrated luminosity with 60% beam polarizations in our beam-use-proposal for Run 9. The Figure-of-Merit (FoM) for gluon polarization measurements scales with the luminosity and the fourth power of the polarization and thus reached only 34% of the goal. The main reasons for this shortfall are a somewhat shorter running period than anticipated, and RHIC luminosity and polarization performance. STAR thus intends to return to 200 GeV polarized proton operations in a future year to complete the longitudinal and transverse physics program at this energy.
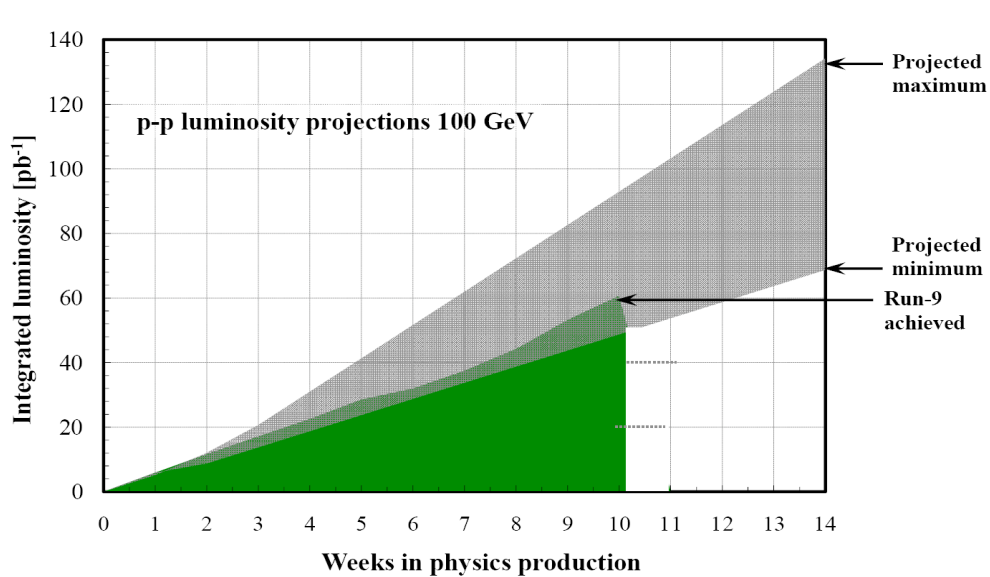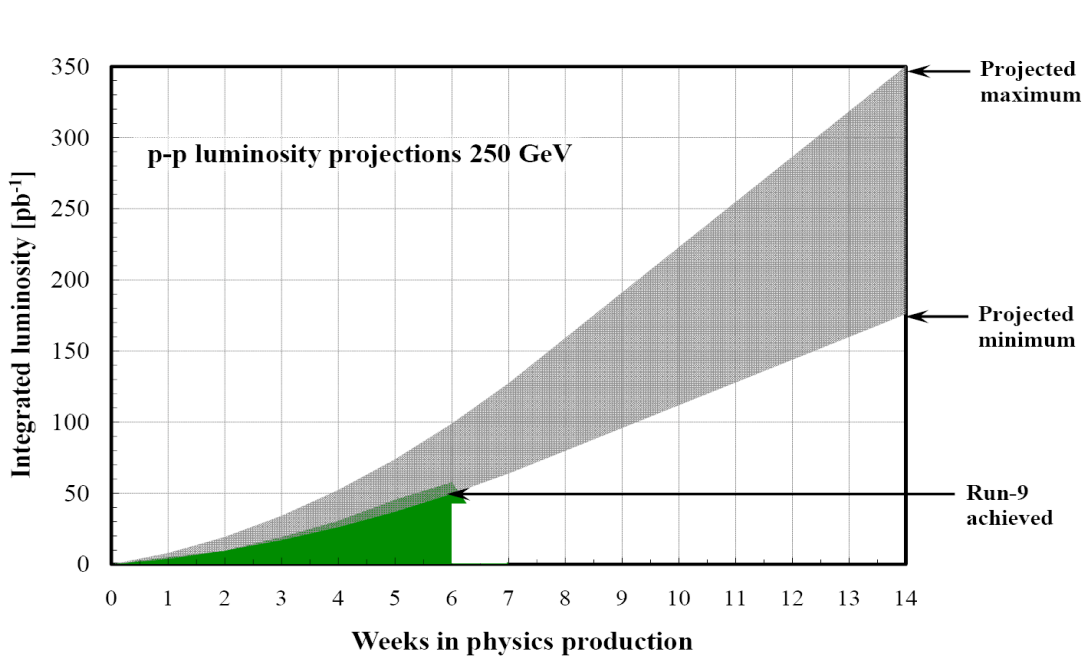

Figure 4.1: RHIC Run 11 polarized proton luminosity projections for 100 GeV running. The expected store polarization is 50-65% and average store luminosity is up to 30x10^{30} cm^{-2} s^{-1}. This graph assumes that minimum peak performance is achieved from the beginning and the maximum peak performance after 4 weeks of linear ramp-up.

A task force of RHIC accelerator personnel headed by Wolfram Fischer, have updated detailed estimates of future polarized proton performance for both $\sqrt{s}$ = 200 and $\sqrt{s}$ = 500 GeV collision energies based on past experience and expectations of future improvements

in operations and hardware. These projections for Run 11 are summarized in figures 4.1 and 4.2 below for 100 and 250 GeV proton beam energies.

The RHIC estimates take into account the following planned upgrades: the AGS horizontal tune jump, modification to the beam dump system, the 9 MHz RF system and changes to the acceleration scheme in RHIC near the 2/3 working point. The assumptions for luminosity ramp-up are listed in the figure captions.

Figure 4.2: RHIC Run 11 polarized proton luminosity projections for 250 GeV running. The expected store polarization is 35-50% and average store luminosity is up to 100×10^{30} cm^{-2} s^{-1}. Higher polarizations may require a new working point. These estimates assume that peak performance is reached after 8 weeks of linear ramp-up, starting with 25% of the final value.

The planned upgrades are briefly explained as follows: The AGS horizontal tune jump is expected to address issues with the intensity-dependence of polarization in the AGS. Tests in 2009 and 2010 indicate that this may result in up to 5% more polarization. A 20% increase in allowable intensity is expected from an increase in the kicker strength as part of the beam dump system. A sharp drop in polarization during ramping for the yellow beam has been investigated. It was found that better transmission was obtained for fewer bunches with the same intensity, which points to electron clouds as the probable source of the problem. The 9 MHz RF system is intended help reduce losses of greater than 15% currently observed in the yellow beam during ramping. Polarization and luminosity performance are limited by beam-beam interactions, which in turn lead to tune spread of particles in the transverse direction. In Run 8 and Run 9, a new near-integer working point was studied which would allow for a larger tune spread and better transmission of polarization through the ramp. However, these studies uncovered a 10 Hz mechanical vibration in the magnet lattice which limits the stability of this working point. A feedback

system has now been tested to minimize these oscillations and allow RHIC to operate at this working point.

As seen in Figures 4.1 and 4.2, delivered luminosity is expected to increase significantly during the course of the run. Beam polarizations are expected to develop more modestly. It should be kept in mind, however, that increases in beam polarization generally lead to large changes in FoM, in particular when beam polarization values are not large. An increase from 35% to 50% beam polarization, for example, doubles the FoM for single-spin measurements and quadruples the FoM for double-spin measurements. We note, furthermore, that high polarization values are advantageous in reducing systematic uncertainties in spin measurements and consider polarization development at $\sqrt{s}$ = 500 GeV in Run 11 a high priority.

The RHIC projections for Run 11 and Run 12 polarized protons are summarized as follows:

Run 11 - 500 GeV

Maximum Luminosity:	85-160 10^{30}cm^{-2} s^{-1}
Average Luminosity:	55-100 10^{30}cm^{-2} s^{-1}
Integrated Luminosity:	18-30 pb^{-1}/wk
Average Polarization:	35-50%

Run 12 - 500 GeV

Maximum Luminosity:	85-250 10^{30}cm^{-2} s^{-1}
Average Luminosity:	55-150 10^{30}cm^{-2} s^{-1}
Integrated Luminosity:	18-50 pb^{-1}/wk
Average Polarization:	35-55%

Run 12 - 200 GeV

Maximum Luminosity:	50-55 10^{30}cm^{-2} s^{-1}
Average Luminosity:	25-30 10^{30}cm^{-2} s^{-1}
Integrated Luminosity:	8-10 pb^{-1}/wk
Average Polarization:	55-65%

For our physics goals, we assume a mid-point of the projected minimum and maximum delivered integrated luminosities, and scale by 60% to account for the anticipated STAR data sampling efficiency. We consider of particular importance also the development of beam polarization, and consider it essential for the success of the $\sqrt{s} = 500$ GeV longitudinal spin physics program to measure (anti-)quark polarizations and gluon polarization that proton beam polarizations of 50% or more, at the high end of or exceeding the RHIC Collider Projections, are achieved routinely and reproducibly during physics production running towards the end of Run 11.

4.3. Experience and Progress from Run 9

Run 9 began with 10 weeks of RHIC operations to develop and establish polarized proton collisions at $\sqrt{s} = 500$ GeV center-of-mass energy. About 5 weeks were available for physics. Our goals included the commissioning and operation of STAR in the $\sqrt{s} = 500$ GeV environment including, in particular, the development of local polarimetry for transverse polarization components at the STAR IP. In addition, we aimed to measure the W production cross section in the leptonic channel as well as a first longitudinal spin asymmetry A_L provided that sufficient luminosity and polarization could be achieved. We report our progress on each of these in sections 4.3.1-3.

Run 9 continued with a period of physics production at $\sqrt{s} = 200$ GeV with the primary aim to record 50 pb^{-1} with average longitudinal beam polarizations of 60%, corresponding to a FoM of 6.5 pb^{-1} to advance our understanding of the gluon polarization, Δg, based on measurements of inclusive jets and other hard probes and on measurements of di-jet and photon-jet correlations to map the kinematic dependence, $\Delta g(x)$. This program is a continuation of our measurements in Run 6 and before. As described in section 4.2, the recorded FoM is well below the goal even though it represents a significant advance over Run 6. No progress was made in Run 9 on transverse physics goals at $\sqrt{s} = 200$ GeV. The offline reconstruction of Run 9 data has just completed and physics analyses have been started. We aim to return to and complete the $\sqrt{s} = 200$ GeV longitudinal and transverse spin physics program in Run 13.

Run 9 concluded with 1 week of data taking at $\sqrt{s} = 200$ GeV with transverse beam polarizations and dedicated beam optics settings for measurements of elastic scattering and central production in double-Pomeron exchange using the Roman Pot instrumentation of the former pp2pp experiment, which is now integrated in STAR. Our progress is reported in section 4.3.4.

4.3.1. Polarimetry at the STAR IP

Polarimetry is an essential component of spin measurements. A polarized hydrogen-jet target is used at IP 12 to measure absolute beam polarizations while a series of Carbon-Nuclear-Interference polarimeters monitor the relative beam polarizations many times over the course of a store. Spin rotator magnets upstream and downstream of the STAR IP are powered to direct the beam polarizations during longitudinal spin physics production runs. Monitoring of transverse polarization components at the STAR IP is especially important

during these times. Local polarimeters provide feedback to CAD regarding the performance of the spin-rotator magnets and monitor any residual transverse beam components.

At $\sqrt{s}$ = 200 GeV, STAR has routinely used Beam Beam Counters (BBCs) as local polarimeters. The BBCs are integrated into a scaler system and real-time analysis of the data provides statistically significant asymmetry measurements within 10 minutes. At $\sqrt{s}$ = 500 GeV, however, the BBCs do not show an appreciable analyzing power and are no longer useful alone as an online local polarimeter. For this reason, STAR commissioned the Zero Degree Calorimeter Shower Maximum Detector (ZDC SMD) during Run 9 for use as a local polarimeter.
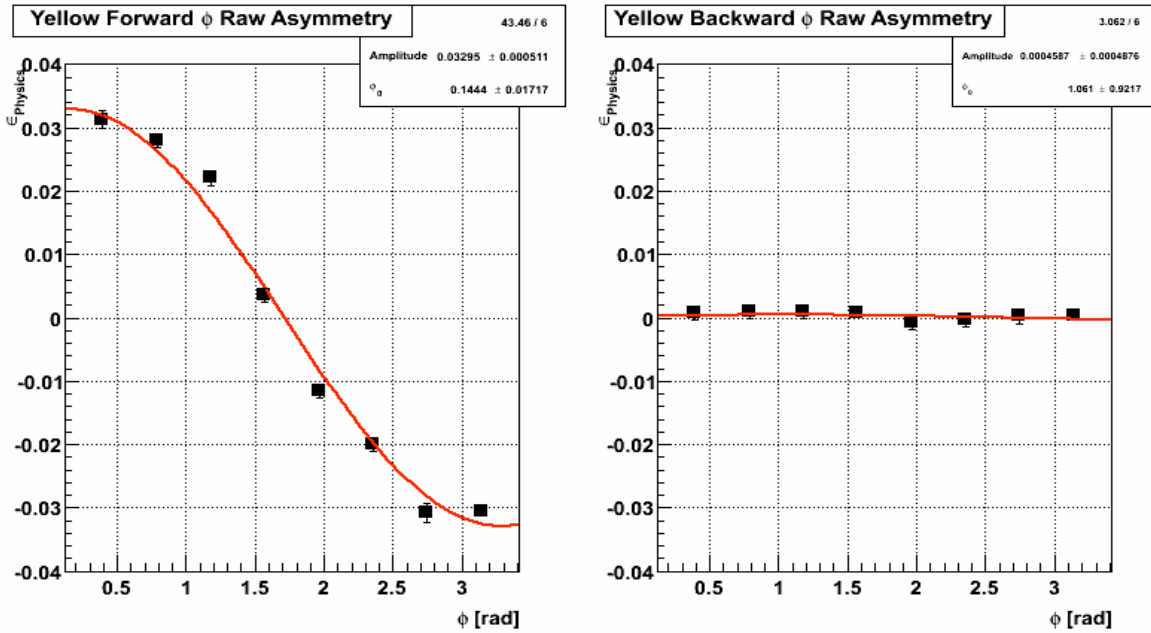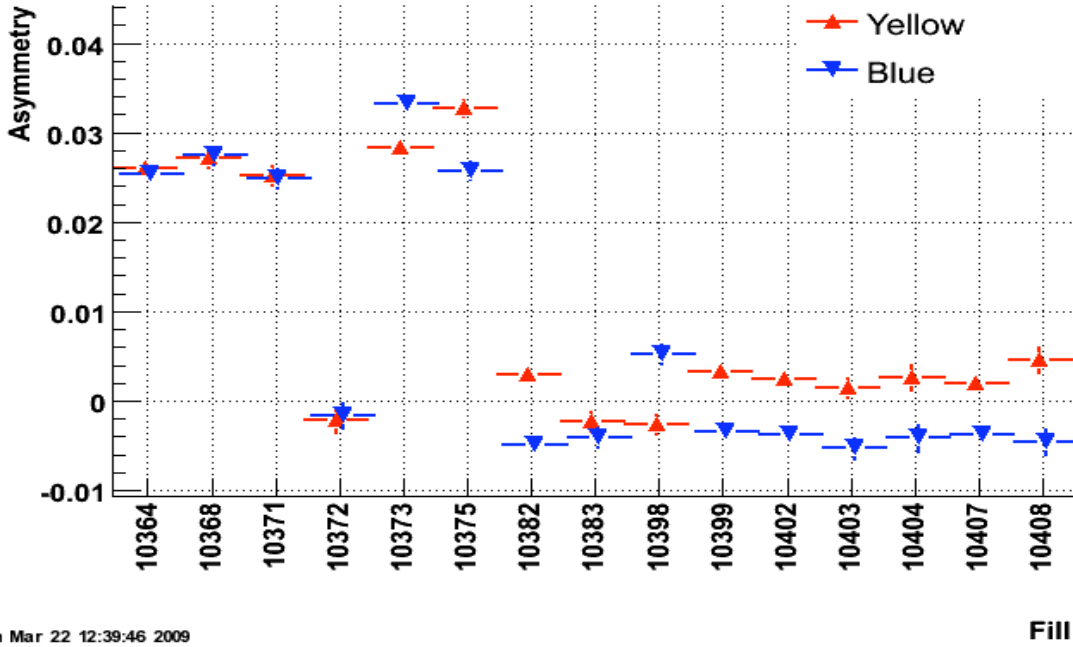

Figure 4.3: Left-right single-spin asymmetries as a function of azimuthal angle for particles detected in the ZDC SMD.

During the transverse running period of Run 9, various trigger conditions for ZDC SMD polarimetry data taking were tested. The triggers varied in the requirements placed on the BBCs and thresholds in the ZDC calorimeter modules. Data taken with a trigger which required a coincidence of BBC energy deposited in the small tiles on both the east and west sides of the interaction region, and moderate energy deposited in the front and back ZDC calorimeters on either the east or west side of STAR showed an analyzing power of approximately 8% for both beams. This result was verified by two independent analyses. The forward and backward left-right asymmetries as a function of azimuthal angle for the yellow beam are shown below. These data were taken with the trigger described above.

The analysis algorithms have been implemented in online monitoring of the ZDC SMD asymmetries. This monitoring made results available within minutes after a run was taken. The asymmetries from this online analysis are shown in the figure below. Note that fill

10372 was intentionally un-polarized and fill 10382 marks the beginning of the longitudinal beam running.

Figure 4.4: Left-right single-spin asymmetries as a function of fill number as recorded with ZDC SMD online monitoring.

The measurements with the ZDC-SMD were key in establishing longitudinal polarization directions in $\sqrt{s} = 500$ GeV collisions at the STAR IP and serve to quantify systematic uncertainties associated with residual transverse beam components in the longitudinal spin asymmetry measurements.

Since the completion of the data taking in Run 9, we have begun an investigation of the physics cause of the large asymmetries observed with the ZDC SMD. We have observed the following features in the data which were triggered as described above:

a) The BBC on the same side as the ZDC which fired the trigger with a hit in the ZDC front and back calorimeter modules has a lower multiplicity of hits in the inner tiles than the opposite side.

b) The BBC shows an appreciable analyzing power at $\sqrt{s} = 500$ GeV if a hit in the ZDC on the same side of the interaction region is required.

c) An asymmetry which combines information from the ZDC and BBC detectors is larger than the asymmetry using the ZDC alone.

These characteristics may arise if the observed asymmetry has its origins in a low multiplicity (low mass) diffraction dissociation process, as predicted and qualitatively confirmed by simple Monte Carlo models.

STAR aims to replace the aged ZDC modules before Run 11 and integrate the ZDC polarimeter into a similar scaler system as used for the BBC polarimeter. Various algorithms for the scaler implementation are currently being tested with existing data. We additionally plan on taking a modest amount of regular data to further investigate the physics cause(s) of the large observed asymmetries. This would be done at all available collision energies and would make use of other STAR instrumentation, potentially including even the (existing or planned) Roman Pot setup.

4.3.2. W Cross-section and Asymmetry A_L

The initial data sample from polarized proton+proton collisions $\sqrt{s}$ = 500 GeV in Run 9 has been analyzed. The detector systems used in this analysis are the STAR Time Projection Chamber (TPC), the STAR Barrel Electromagnetic Calorimeter (BEMC) and STAR Electromagnetic Endcap Calorimeter (EEMC). Only the calorimeter tower response has been taken into account in this analysis. The BEMC was used to measure the transverse energy, E_T, of the decay $e^{\pm}$. The suppression of the QCD background by several orders of magnitude was based on the TPC, BEMC and EEMC. Figure 4.5 shows event displays from the 2009 data taking period for a W candidate event (a), a Z^0 candidate event (b) and a di-jet candidate event (c). A lego plot is shown in Figure 4.6 displaying the BEMC E_T and the TPC p_T distribution for a W candidate event at the top and a di-jet candidate event at the bottom.

2009 STAR Data ($\sqrt{s}$=500GeV)

W candidate event Z^0 candidate event   Di-Jet candidate event
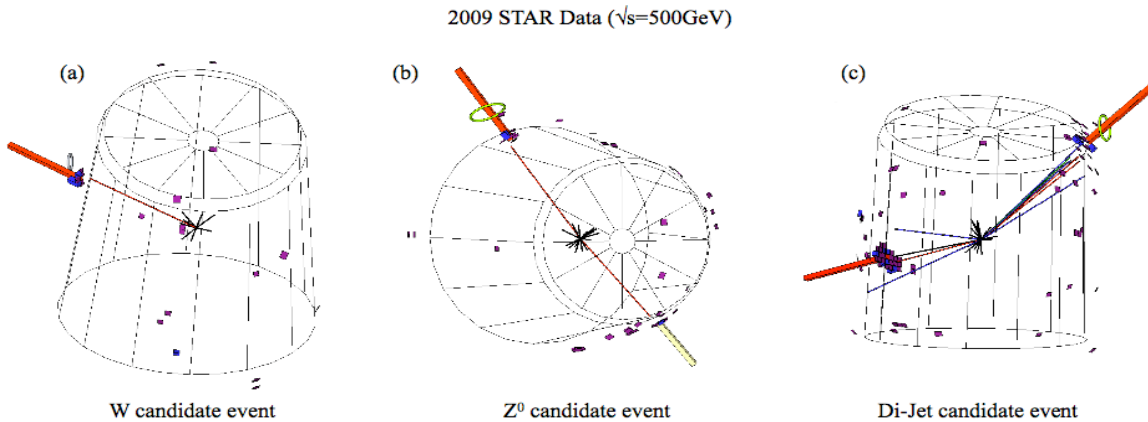
Figure 4.5: Event displays from the 2009 data taking period at $\sqrt{s}$=500GeV showing a candidate event (a), a Z^0 candidate event (b) and a di-jet candidate event (c).

Proton-proton collision events focusing on W production at $\sqrt{s}$ = 500GeV were identified by a two-step energy requirement in the BEMC. Electrons and positrons from W production at mid rapidity are characterized by large E_T peaked at $M_W/2$ (Jacobian peak). At the hardware trigger level (L0), a high tower (HT) calorimetric trigger condition required E_T >7.3GeV in

a single BEMC tower. At the software trigger level (L2), a dedicated trigger algorithm was developed that required that a 2 X 2 tower cluster E_T sum exceeds 13GeV. The offline selection of W candidate events is based on kinematical and topological difference between leptonic $W^{\pm}$ decays, and QCD background events as shown in Figure 4.5 and Figure 4.6. Events from $W^{\pm} \rightarrow e^{\pm} + \nu$ decays contain a nearly isolated $e^{\pm}$ with a neutrino in the opposite direction in azimuth. The neutrino escapes detection, leading to a large missing energy.
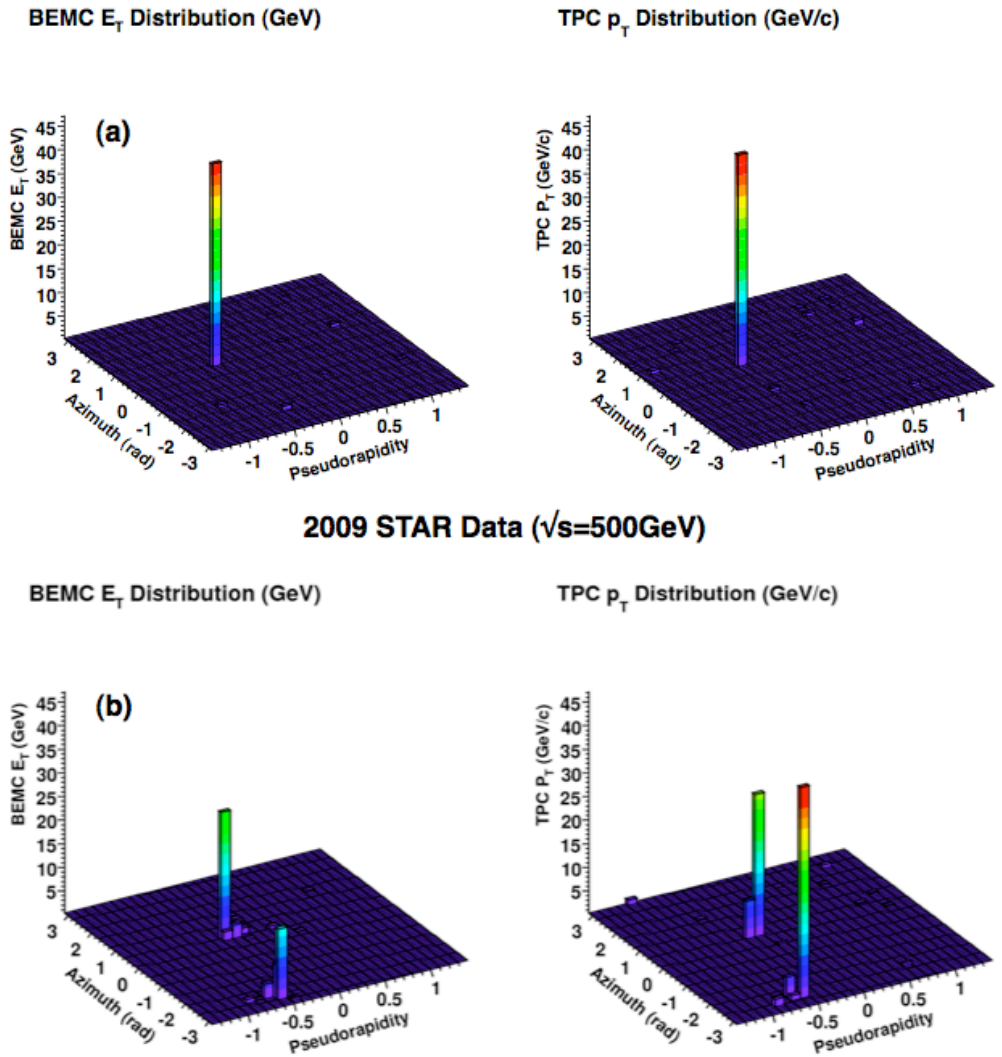
Figure 4.6: Lego plot showing the BEMC E_T and the TPC p_T distribution for a W candidate event (a) and a di-jet candidate event (b).

Figure 4.7 illustrates the basic idea of the selection of W candidate events. The 2D histograms show for one W candidate event the TPC p_T (a) and the BEMC tower E_T (b) distribution along with both BEMC shower-maximum detector (SMD) layers (c) / (d) as a function of the azimuthal angle φ and the pseudo-rapidity η. The approximate area of a 2x2

tower cluster is indicated by a small circle around the large energy deposition in a single BEMC tower. Also shown is the size of a cone (near-cone) around the electron candidate. The away-side area is sketched by the black dashed rectangular region. The TPC high-p_T entry appears in the same η-φ region as the large BEMC E_T entry. Both BEMC SMD layers show a large energy deposition at the same location in the η-φ plane as the TPC high-p_T and the BEMC high-E_T entry.
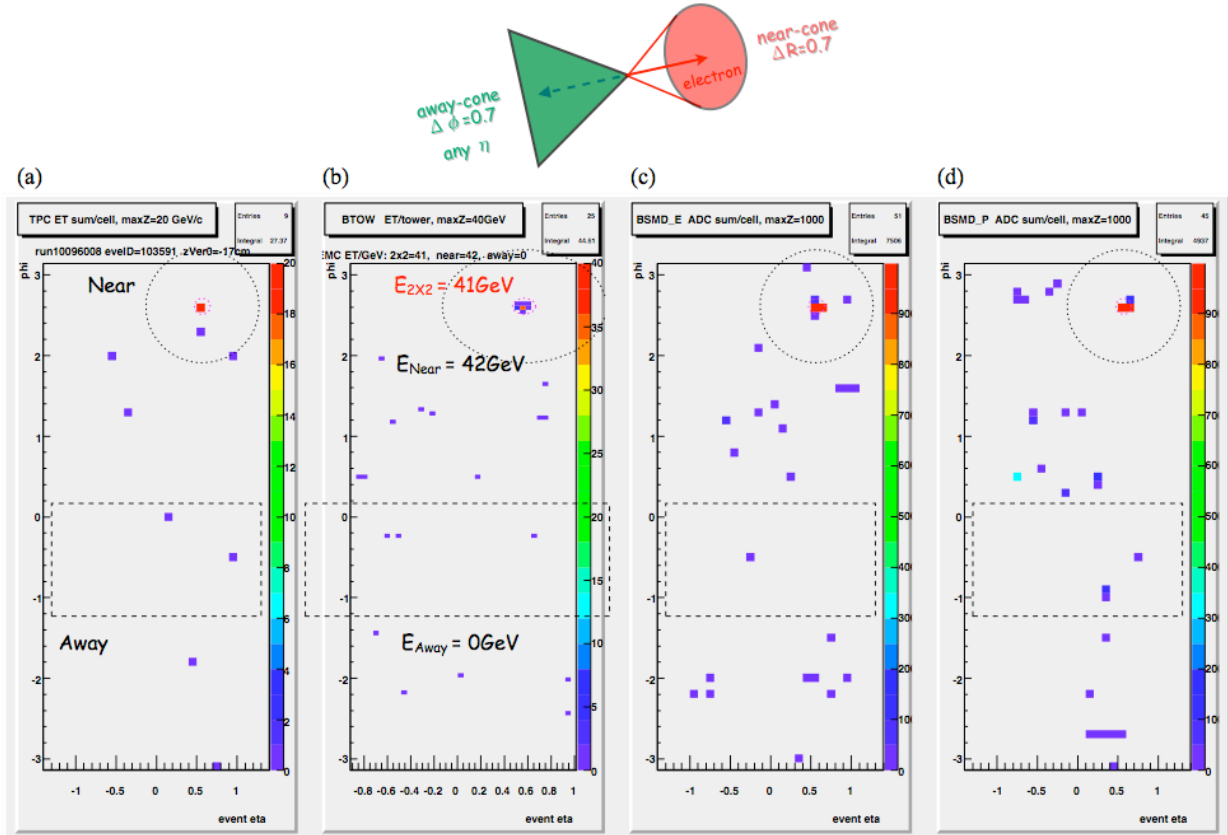
Figure 4.7: Illustration of the W offline selection criteria (top) and the distribution of the TPC p_T (a) the BEMC E_T (b) and both BEMC SMD layers (c) / (d) in azimuth and pseudo-rapidity.

An electron candidate is defined to be any TPC track with p_T>10GeV/c that is associated with a primary vertex with |z|<100cm, where z is the distance along the beam direction.

A 2x2 BEMC tower cluster E_T sum is required to be larger than 15GeV. The excess BEMC E_T sum in a 4 X 4 tower cluster centered around the respective 2 X 2 tower cluster is required to be below 5%. In addition, the distance between the 2 X 2 cluster tower centroid and the TPC track is required to be less than 7cm. A near-cone is formed around the electron candidate direction with a radius in η-φ space of R=0.7. The excess BEMC and TPC E_T sum is required to be less than 12% of the 2 X 2 cluster E_T. The away side requirement is based on a cut on the BEMC and TPC E_T sum to be less than 8GeV. This sum is extended over the full η range of the BEMC and EEMC and Δφ=0.7 as shown in

Figure 4.7. Figure 4.8 shows the evolution of all cuts for the BEMC 2 X 2 E_T distribution. A clear Jacobian peak emerges characteristic for W production in contrast to QCD background dominating the low E_T region.
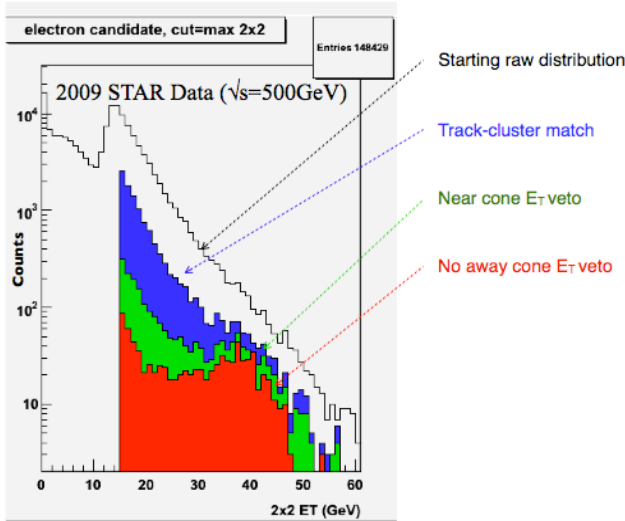

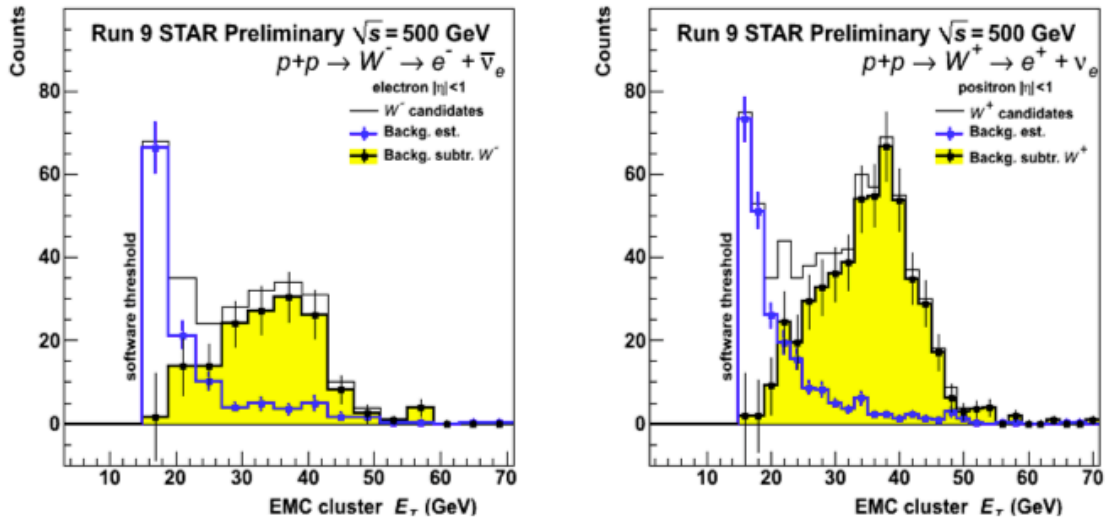**Figure 4.8: Evolution of W offline selection cuts (See text for further details).**

Figure 4.9: E_T for W⁻ (left) and W⁺ (right) events.

Figure 4.9 presents the charge-separated lepton E_T distributions based on the selection criteria given above. W candidate events are shown as the black histograms, where the characteristic Jacobian peak can be seen at approx. $M_W/2$. The total number of candidate events for $W^{+(-)}$ are 459 (151) for $25 < E_T < 50$GeV. A data-driven procedure was applied to estimate the level of QCD background events. The first part consists of an estimate of the impact of the missing calorimeter coverage for $-2 < \eta < -1$ on the cluster E_T distribution. This estimate was obtained by performing a parallel analysis without the EEMC as an active detector. The difference in yield of accepted events as a function of E_T provides an absolute

estimate for the missing calorimetric coverage. The remaining background is estimated by fitting a separate QCD shape distribution in E_T to the region of $E_T < 19 GeV$.
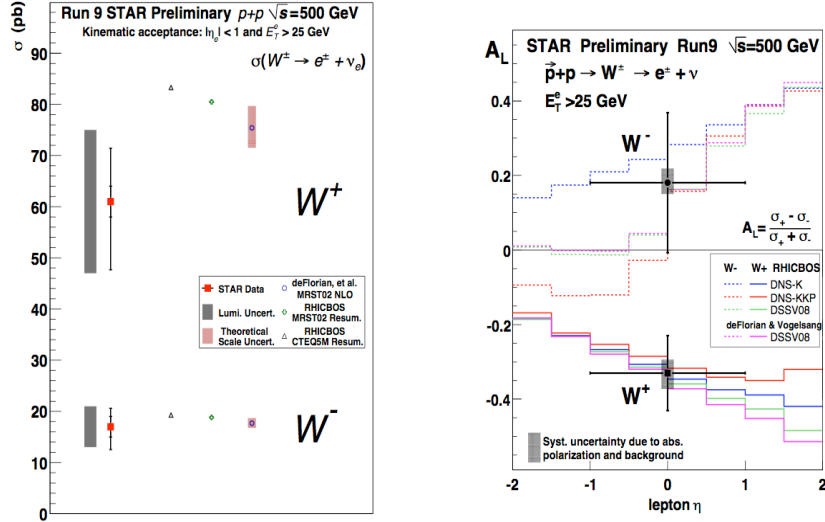
Figure 4.10: Preliminary results on the production cross section, and on the longitudinal single-spin asymmetry for $W^{\pm}$ events as a function of lepton η.

The measured A_L was computed from $W^{\pm}$ candidate events with $25 < E_T < 50 GeV$ and $|\eta| < 1$. Figure 4.10 shows the measured asymmetries $A^{W+}_L = -0.33 \pm 0.10$ (stat.) ± 0.04 (syst.) and $A^{W-}_L = 0.18 \pm 0.19$ (stat.) $^{+0.04}_{-0.03}$ (syst.) for $|\eta| < 1$ and $25 < E_T < 50$ GeV. The systematic uncertainties of $A^{\pm}_L$, shown as grey bands in Figure 4.10, are dominated by the absolute scale uncertainties of the beam polarization, which amounts to 9.2% for the polarization sum $(P_1 + P_2)$.

Figure 4.10 shows preliminary results for the measured cross sections and asymmetries of $W^{\pm} \rightarrow e^{\pm} + \nu$ from candidate events with $|\eta| < 1$ and $E_T > 25$ GeV in comparison with theoretical expectations based on full re-summed [2] and NLO [3] calculations with different sets of parton distribution functions. The measured cross section is in reasonable agreement with theoretical expectations, which thus provides a benchmark for count rate estimates in future measurements. The re-summed calculations for A_L have been evaluated for the DNS [4] and DSSV [5] set of PDFs, and the former is shown for two different sets of fragmentation functions. The NLO predictions are only shown for the DSSV polarized PDFs. The spread of polarized PDFs in Figure 4.10 encompasses the uncertainty bands as evaluated in the DSSV global analysis [5]. Our A_L results are consistent with predictions using polarized PDFs constrained by inclusive and semi-inclusive pDIS measurements, exhibiting the expected universality of polarized PDFs.

4.3.3. Trigger and Rate Capabilities

The STAR trigger system includes a hardware decision at Level-0 (L0), followed by software triggers at Levels 2 (L2) and 3 (L3). The L0 trigger determines the actual event read-out rate. The L2 and L3 triggers then provide opportunities to reject events, thereby

reducing both the storage requirements and the off-line event production time, and/or identify potentially interesting events for fast off-line analysis. Since the completion of DAQ1000 before Run 9, two things have limited the maximum possible L0 trigger rate. In the past, a few TPC gating-grid high voltage supplies have failed when fired at rates in excess of 2 kHz. The number of spares available has been quite limited, so we have imposed a limit of 700 Hz to be very conservative. More spares will be available by Run 11. The other constraint involves the total charge deposited on the TPC anode wires while the gating grid is open. This limit was also set very conservatively during Runs 9 and 10. Tests late in the Run 10 $\sqrt{s}$ = 200 GeV Au+Au period demonstrated that much higher anode currents can be tolerated without short-term problems (e.g., tripping). The impact of the total long-term integrated anode charge on the TPC lifetime is under investigation. In the middle of the $\sqrt{s}$ = 500 GeV proton+proton period of Run 9, we reduced the high voltage on the TPC inner anode wires from 1170 V to 1135 V, which reduced the gain to ~2/3 of the original value. We have operated the TPC at this reduced voltage without problems throughout the rest of Run 9 and all of Run 10. Additional options to extend the life of the TPC are being considered, such as further reductions in the operating voltage or replacements of the TPC sectors as they age.

During Run 9, the L0 *W*-trigger required that there be at least one BEMC tower with E_T >~ 7.3 GeV. It fired at rates up to ~35 Hz. At L2, the events were also required to have at least one 2x2 cluster of BEMC towers above E_T >~ 13 GeV. Only about one in six L0 triggers passed this additional requirement. The L2 selection facilitates faster off-line analysis of the data. We will include a jet patch (JP) requirement in the L0 trigger, beginning in Run 11. This will introduce a cluster threshold requirement at L0, thereby shifting a fraction of the current L2 rejection to L0 with no impact on the trigger efficiency. The L0 trigger rate could be decreased significantly – with no impact on the efficiency for detecting *W*s – by increasing the high-tower threshold. However, this would require replacing PROMs to change the FPGA programming in all of the BEMC and EEMC front-end electronics, so we don't plan to do this in the near term.

Jet and di-jet cross sections are quite large at 500 GeV. Photon and γ+jet cross sections are much smaller. However, the trigger rates for the latter are dominated by the high rate of π^0 events that look like photons at L0. Thus, optimizing the total L0 trigger rate within the available bandwidth is a very important consideration for gluon polarization measurements at 500 GeV.

During Run 9, we triggered on jets with a newly integrated system of BEMC+EEMC based jet patches. The scheme prior to Run 9 consisted of 18 jet patches, each of size $\Delta\eta \times \Delta\varphi = 1 \times 1$, covering the regions -1 < η < 0, 0 < η < 1, and 1 < η < 2. The new scheme includes these 18 jet patches, plus an additional 12 jet patches covering the regions -0.6 < η < 0.4 and 0.4 < η < 1.4. The overlapping patches significantly reduced previous trigger inefficiencies near η = 0 and 1. For the 500 GeV period of Run 9, we used a JP1 trigger with a threshold at ~8.3 GeV (prescaled) and a JP2 trigger with a threshold at ~13 GeV (not prescaled). Lower energy (di-)jets are the most interesting for gluon polarization measurements during 500 GeV running, as the higher x_g region that is sampled by higher energy (di-)jets is covered more effectively with 200 GeV data. Thus, for Run 11 and

beyond, we plan to add a JP0 jet patch trigger with a threshold at ~6.4 GeV, and then increase the JP1 and JP2 thresholds to rebalance the rates.

During Run 9, we triggered on photon and π^0 events by requiring a high tower above one threshold in coincidence with a jet patch above a higher threshold, equivalent to the scheme that we plan to implement for *W*-triggers in the future. This worked well. However, the higher luminosities anticipated in Runs 11 and 12 will necessitate increasing the thresholds, which would reduce the photon detection efficiency. We are investigating alternatives in an effort to preserve the photon efficiency within the available L0 bandwidth.

We have used the trigger rates that were observed at $\sqrt{s} = 500$ GeV during Run 9 to estimate *W*, (di-)jet, and photon trigger rates for Runs 11 and 12.

4.3.4. Elastic Scattering and Central Production in Double-Pomeron Exchange

During Run 9 one week was used with large ß* beam optics settings to take data on proton elastic scattering with transversely polarized beams at $\sqrt{s} = 200$ GeV in the region of small four-momentum transfer *t*, $0.005 < |t| < 0.035$ (GeV/c)^2, using the Roman Pot setup of the former pp2pp experiment as it is presently installed at the STAR IP. In addition to the elastic scattering data sample, data were recorded with particles in the central region of STAR. Both reactions occur via the exchange of one or more colorless objects with the quantum numbers of the vacuum, historically called Pomerons. The analysis efforts have focused on elastic scattering and central production in double-Pomeron exchange.
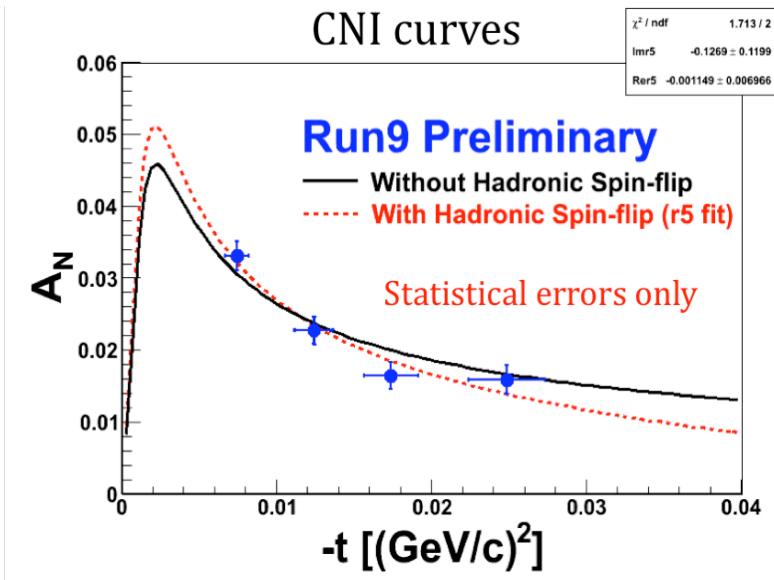

Figure 4.11: Preliminary results in A_N, statistical errors only, a 10 percent t-scale uncertainty was assumed to account for systematic errors due to alignment and transport uncertainty.

In elastic scattering, we have obtained preliminary results of the single spin analyzing power A_N in the Coulomb Nuclear Interference (CNI) region. Figure 4.11 shows the A_N dependence on *t*, where about 15% of the data was used. Shown are statistical uncertainties only. Systematic uncertainties due to alignment and transport are estimated to result in an uncertainty of 10% in *t*.

For central production we are studying final states with two and four charged pions. Figure 4.12 shows the invariant mass distributions of the $\pi^+\pi^-$ and $\pi^+\pi^-\pi^+\pi^-$ final states reconstructed for events recorded with the Central Production triggers, using online conditions on the Roman Pots and the multiplicity in the Time-of-Flight system. The tracks in the STAR TPC were reconstructed offline as were two tracks in the Roman Pots to confirm the trigger condition. The invariant mass M_x was calculated under the assumption that the tracks are all pion tracks.
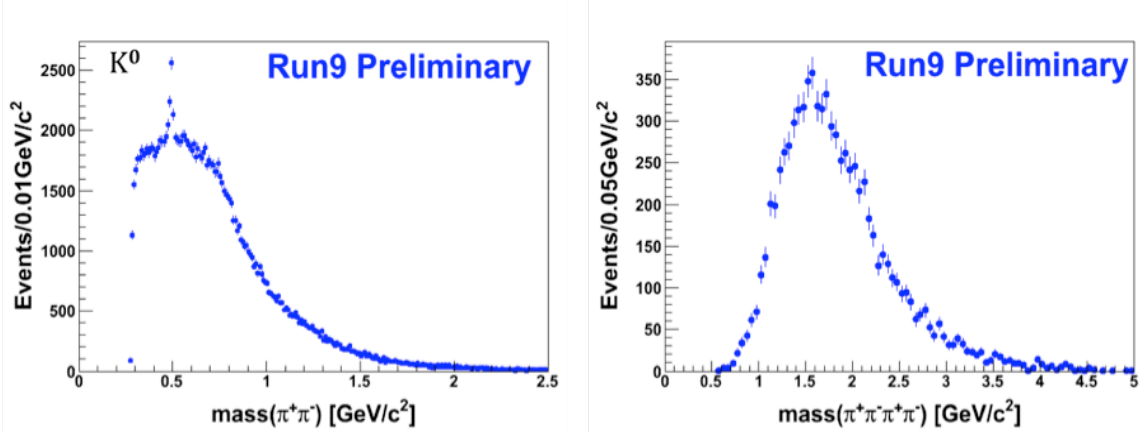
Figure 4.12: Invariant mass distribution of $\pi^+\pi^-$ final states (left panel) and $\pi^+\pi^-\pi^+\pi^-$ (right panel), tracks in the TPC are assumed to be π^+ or π^-.

The invariant mass distributions show that STAR with the Roman Pot upgrade is well suited for physics with tagged forward protons. Significantly more statistics is needed to be able to interpret the invariant mass distributions. For this reason and to measure elastic scattering to larger values of $|t|$, we are proposing to take data at $\sqrt{s}$ = 500 GeV, where acceptance is larger and the data sample can be increased by a factor of 6 – 10 during a one week dedicated run.

4.4. Request for Run 11

The STAR polarized proton-proton Beam Use Request for Run 11 serves continued collider and experiment development at $\sqrt{s}$ = 500 GeV, in preparation for physics production runs with high integrated luminosity and high average beam polarization in subsequent running periods. We anticipate that Run 11 will lead also to new transverse spin physics measurements, described in section 4.4.1 below, and improved W measurements, described in section 4.4.2.

4.4.1. Transverse Spin Physics Measurements at $\sqrt{s}$ = 500 GeV

The large values of the transverse single spin asymmetries, A_N, seen in inclusive π^0 and η production at large Feynman x_F in polarized proton collisions at $\sqrt{s}$ = 200 GeV at RHIC have stimulated substantial theoretical development. These transverse spin asymmetries vanish in leading twist perturbative QCD evaluations with collinear factorization, since they require a non-vanishing helicity flip and interference between the real and imaginary

amplitudes. At RHIC conditions, the π^0 spin averaged cross section has been found in fairly good agreement with such calculations at next-to-leading order. Thus, the transverse asymmetries provide a laboratory for sensitive study of non-leading twist aspects of hadron interactions in the hard scattering regime.
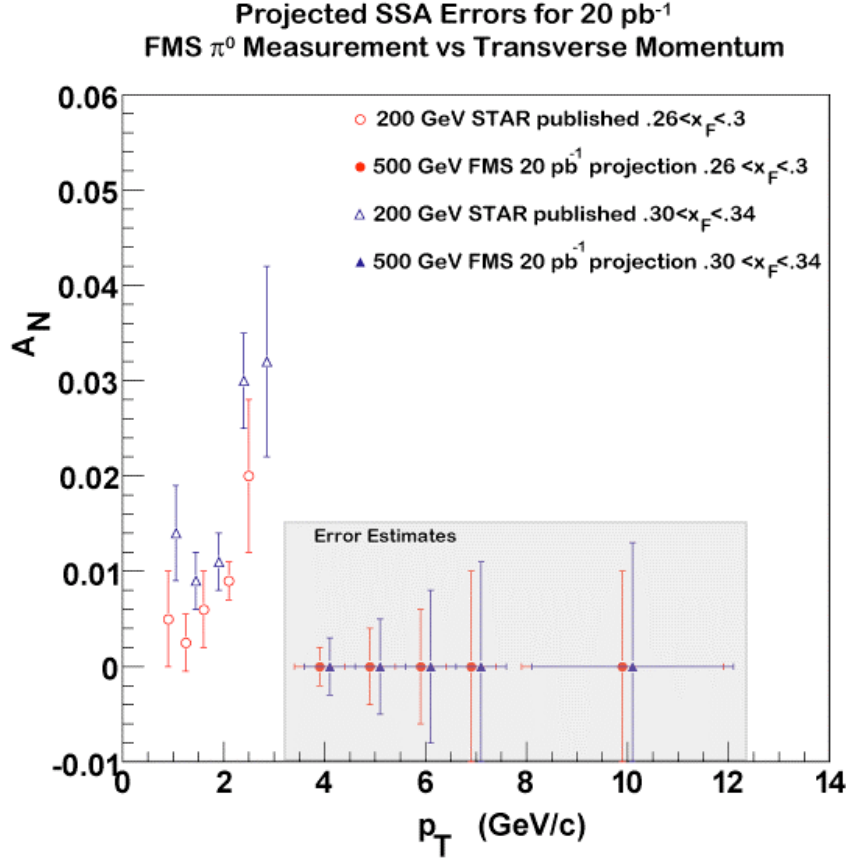
Figure 4.13: Anticipated statistical precision in neutral pion A_N versus p_T at $\sqrt{s} = 500$ GeV for an integrated luminosity of 20 pb^{-1} and a beam polarization of ~60% for indicated x_F compared with published STAR data at $\sqrt{s} = 200$ GeV.

Run 11 presents the next opportunity to significantly advance the knowledge of the π^0, η, and possibly also the photon single transverse spin asymmetries, as well as their scaling properties in x_F, p_T, and $\sqrt{s}$. We propose to use 4 weeks at the beginning of polarized proton operations at $\sqrt{s} = 500$ GeV to sample an integrated luminosity of ~20 pb^{-1} with ~40-45% transverse polarizations, based on the midpoint performance in the RHIC Collider Projections. This data sample would present a qualitative advance over existing measurements. Specifically, we anticipate to be able to measure A_N for π^0 with the STAR Forward Meson Spectrometer in five intervals in the pseudo-rapidity region $2.6 < \eta < 4.1$ by five intervals in x_F in the range $0.2 < x_F < 0.4$ with a statistical precision ranging from 0.004 at smallest x_F to 0.2 at largest x_F and smallest η, and typically with tenfold better precision at largest η. As illustrated in Figure 4.13 for a specific range in x_F, we expect that this sample will allow characterization of the (surprising) p_T dependence of A_N over a broad range up to $p_T \sim 10$ GeV/c with percent level precision, or about twice the range of published data at $\sqrt{s} = 200$ GeV [1]. This data sample should, furthermore, allow

measurement of the asymmetry A_N in the mass region of the η meson at √s = 500 GeV. The projected precision is shown, together with the surprisingly large preliminary values observed at √s = 200 GeV, in Figure 4.14.
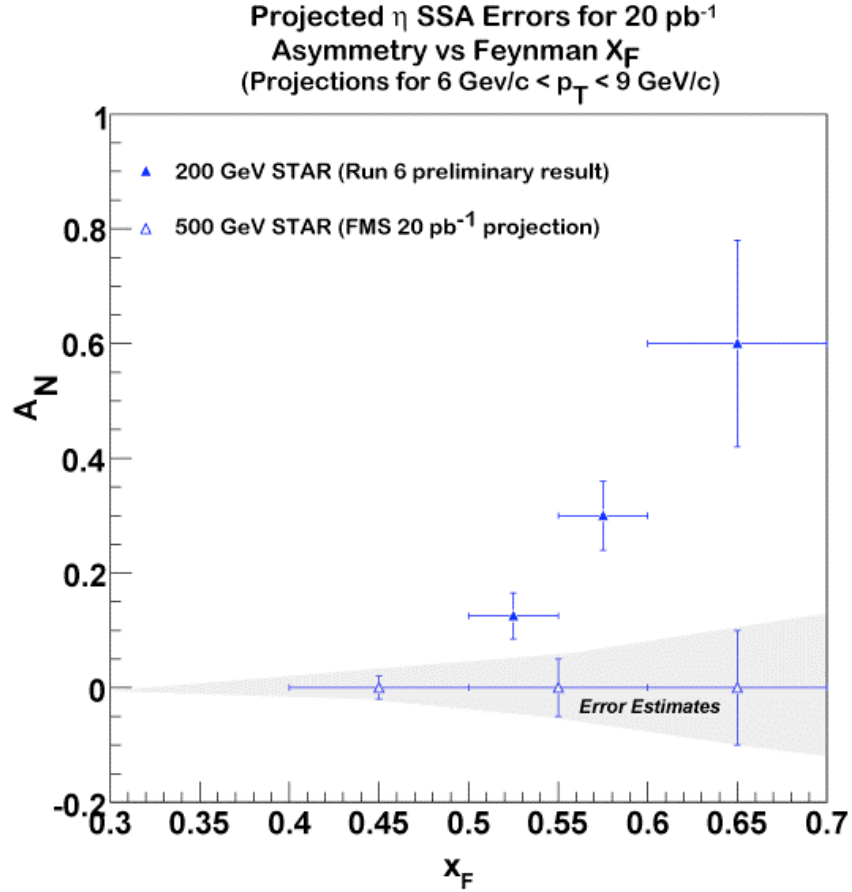
Figure 4.14: Anticipated statistical precision in A_N in the region of the η mass region versus x_F at √s = 500 GeV for an integrated luminosity of 20 pb^{-1} and a beam polarization of ~60% for indicated x_F compared with preliminary STAR data at √s = 200 GeV.

We note that STAR has started to investigate possibilities to upgrade its forward measurement capabilities with hadronic calorimetry and with tracking, even though their physics potential is beyond the horizon of this proposal. The former upgrade aims to enable forward spin physics with (anti-)Λ hyperons and to enhance capabilities for jet-like events, whereas the latter would serve future Drell-Yan transverse spin measurements.

4.4.2. Longitudinal Spin Physics Measurements at √s = 500 GeV

The longitudinal beam use request for Run 11 aims to significantly improve on the first measurements of the longitudinal single-spin asymmetry A_L for W boson production made in Run 9. These measurements will continue to focus on the mid-rapidity region. The extension into the backward and forward rapidity region requires the installation of the STAR Forward GEM Tracker which is expected to take place after Run 11 in Summer

2011. For this reason, and because of the high demands on integrated luminosity and polarization of the measurements, the W program can reach its full potential only after multiple running periods at $\sqrt{s} = 500$ GeV.
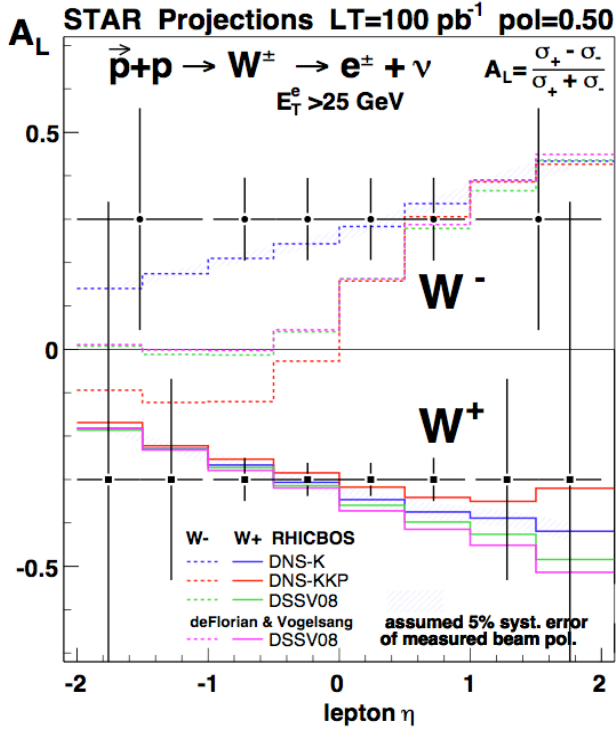

Figure 4.15: Projected A_L sensitivity for a luminosity of 100 pb^{-1} and 50% beam polarization.

Figure 4.15 shows the projected uncertainty in A_L as a function of the electron/positron rapidity for W boson production with $E_T > 25$ GeV based on an initial data sample corresponding to an integrated luminosity of 100 pb^{-1} and a mean beam polarization of 50%, and forms an intermediate goal of the W physics program. Based on Run-9 experience, we have assumed in our uncertainty estimates that the fraction of background events will be the same as in Run-9 data and that the total W reconstruction efficiency at mid-rapidity will be improved from ~55% to ~65%. The theory curves have been discussed before in section 4.3.2.

Measurements of A_L at this intermediate precision will, generally, focus on determining the rapidity dependence over the STAR acceptance region. This will allow to map out different dependencies of A_L on the underlying polarization of quarks and anti-quarks and thus provides meaningful input for a global analysis. Measurements of A_L at mid rapidity will allow a first step in determining the rapidity dependence over four bins as shown in Figure 4.15. It is expected that, at this level of precision, the measurement would start to provide constraining sensitivity to the anti-u quark polarizations for negative lepton rapidities in the case of W^- production.

During the proposed 6 weeks of longitudinally polarized proton operations, following 4 weeks of proton operations with transverse polarizations, RHIC projects to deliver in Run 11 an integrated luminosity in the range of 85 pb^{-1} to 170 pb^{-1} with beam polarizations

between 35% and 50%. STAR is expected to sample 60% of the delivered luminosity and the full magnitude of RHIC polarization, after tuning of the spin rotator magnet currents. The intermediate physics goal presented in Figure 4.15 can thus be achieved with 6 weeks of data taking in Run 11 only if actual RHIC performance will be at the upper end of the projected performance for both luminosity and polarization. Luminosity and polarization performance at the mid-point of the RHIC Collider projections, would result in about half the FoM.

Measurements of double-longitudinal spin asymmetries rely more crucially on actual beam polarization performance than single-longitudinal spin asymmetry measurements at equal precision. In view of the polarization development projected for Run-11 and the expected size of the physics asymmetries A_{LL} for jet and di-jet production at $\sqrt{s}$ = 500 GeV, we anticipate that meaningful A_{LL} measurements will be made starting only in Run 12.

4.4.3. Elastic Scattering and Central Production in Double-Pomeron Exchange

We propose to allocate one week of beam time at $\sqrt{s}$ = 500 GeV with transverse beam polarizations during Run 11 to extend our measurements of the spin dependence of elastic scattering to tenfold larger values of $|t|$. The primary motivation is that, in elastic scattering at $\sqrt{s}$ = 200 GeV, we have measured a significant single spin analyzing power A_N, which is suggestive of a hadronic spin flip contribution. It is of considerable interest to extend this measurement to larger values of $|t|$, which is possible only with higher collision energies. These measurements will furthermore allow to record a 5-10 times larger sample of Central Production events.
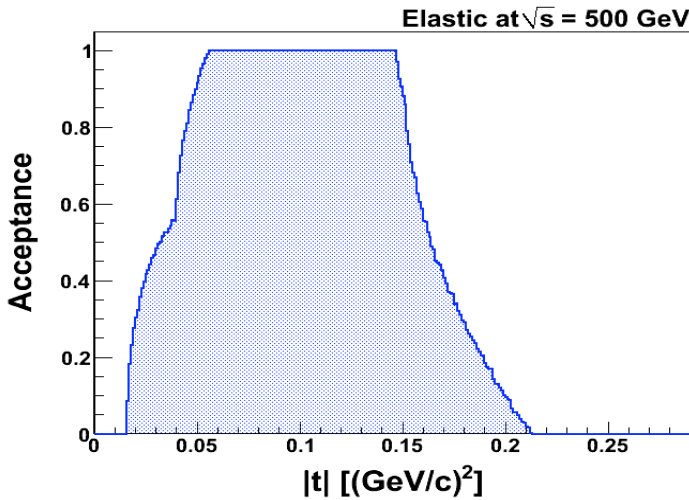
Figure 4.16: Acceptance as function of |t| of the setup proposed for BUR 11 at $\sqrt{s}$ = 500 GeV.

With the current location of the Roman Pots special $\beta^* = 7$ m optics is needed and hence one week of dedicated time beam time is required. This is similar to the request and operations at the end of Run 9, during which one week of very successful, dedicated running at $\sqrt{s}$ = 200 GeV was allocated to taking data with transverse polarization. By using the capacity of existing power supplies optics of $\beta^* = 7$ m at $\sqrt{s}$ = 500 GeV can be produced allowing the $|t|$-range for elastic scattering $0.015 < |t| < 0.2$ $(GeV/c)^2$, as shown in Figure 4.16.

By measuring spin related asymmetries one will be able to determine elastic scattering at the amplitude level [10-13]. In Run 11 we plan to measure A_{NN}, A_{SS}, and A_N at $\sqrt{s} = 500$ GeV. Similar analyses from Run 9 data at $\sqrt{s} = 200$ GeV are on going. The full azimuthal coverage of the elastic events that we have will assure high efficiency and small errors of the measurements.

In addition to spin dependent parameters we will make the first measurements of spin averaged pp elastic scattering at $\sqrt{s} = 500$ GeV. Given Run 9 experience we can expect at least 20×10^6 elastic events could be collected, which would allow precise measurement of the nuclear slope parameter with $\Delta b = 0.31$ $(GeV/c)^{-2}$ and the total cross section with the error $\Delta\sigma_{tot} = 2\text{-}3$ mb, where the biggest contribution is from the systematic error on luminosity measurement.

4.5. Request for Run 12

The installation of the STAR Forward GEM Tracker (FGT) is planned for summer 2011 along with a new inner support structure and beam pipe. Run 12 will be the first run to take full advantage of the charge-sign discrimination capabilities for forward leptonic *W* decay electrons and positrons provided by the FGT. Figure 4.17 shows a side view of the new inner tracking system with the planned Heavy Flavor Tracker (HFT) at the center and the FGT on the right side. Also shown is the new East (left side) and the new West (right side) cylindrical mechanical support structure.

The *W* production cross-section in the STAR EEMC acceptance region of 1<η<2 is much smaller than at mid rapidity. The *W* program at RHIC, in particular in the backward / forward rapidity region is a multi-year program.
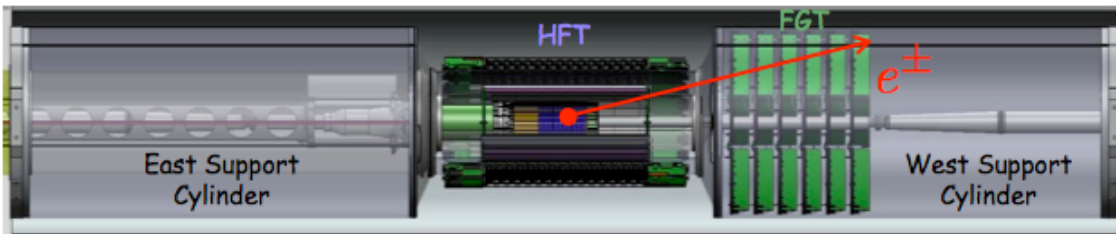
Figure 4.17: Upgrade STAR inner and forward tracking system showing the location of the Heavy Flavor Tracker (HFT) and the Forward GEM Tracker (FGT).

The backward (forward) rapidity region is being accessed depending on the which of the polarized proton beams is being considered moving away (towards) the STAR EEMC to measure the longitudinal single-spin asymmetry for W boson production. Figure 4.18 shows the projected performance for a multi-year program based on a recorded data sample of 300pb^{-1} and a beam polarization of 70%. The projected performance at backward and forward rapidity is based on a rather conservative assumption about the level of signal over background of approximately 1.1. This estimate is based on a full QCD background MC simulation. Assuming that the Run 9 performance of signal over background of approximately 10 at mid rapidity could be also achieved for the backward/forward rapidity

region, a reduction of almost a factor two in the achievable uncertainty can be expected. The impact of a large W data sample of similar size as above constraining anti-u and anti-d quark polarizations has recently been shown by a global fit analysis assuming projected data from STAR and PHENIX.
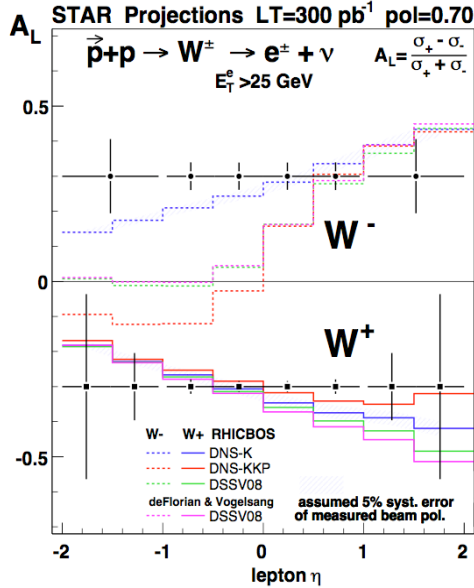

Figure 4.18: Projected A_L sensitivity for a data sample of 300pb^{-1} and 70% beam polarization.
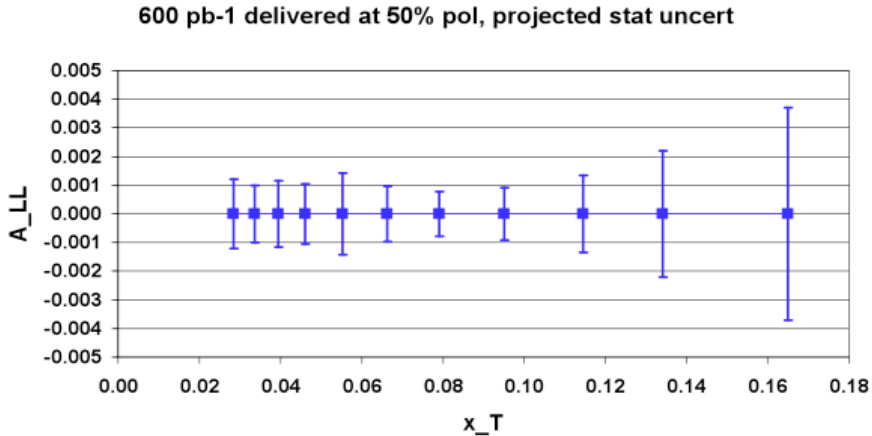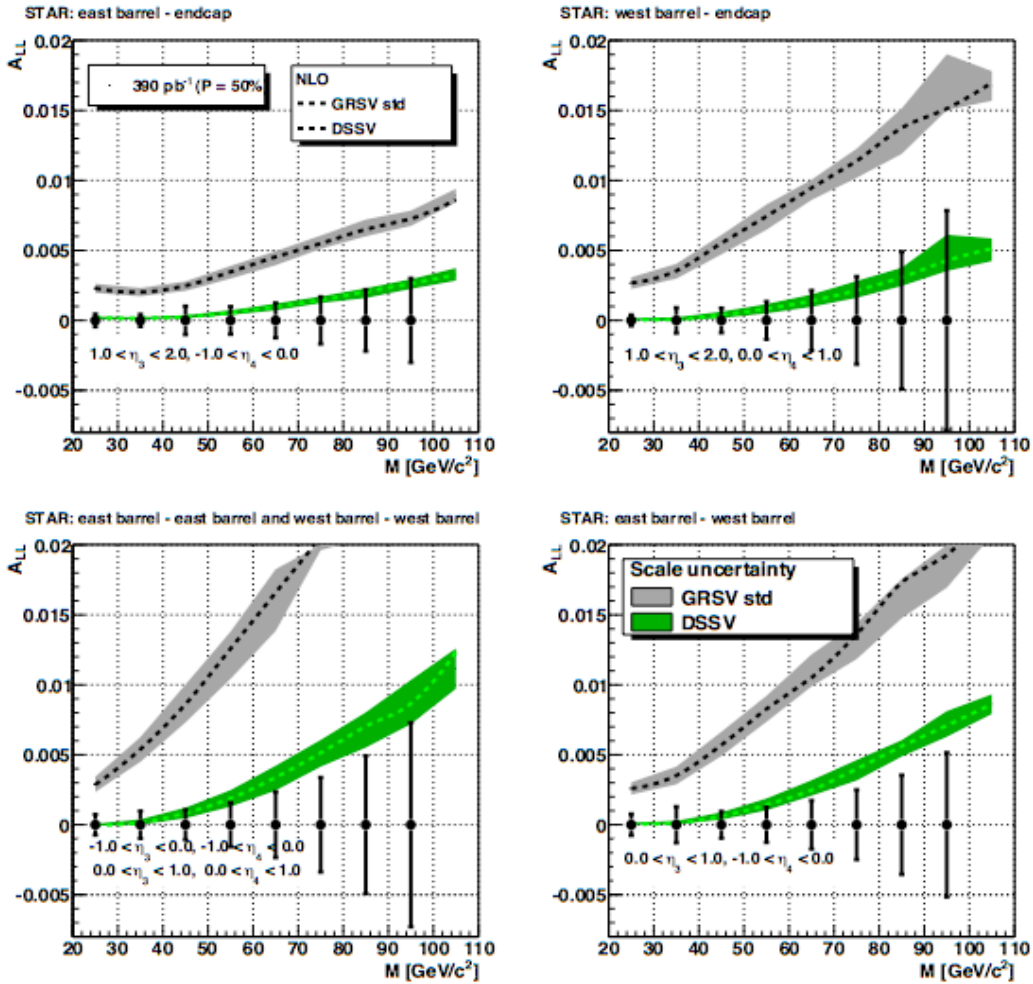

Figure 4.19: Projected A_{LL} for inclusive jet production for a large, multi-year, 500GeV data sample as function of x_T.

In addition to the *W* physics program, the 500GeV polarized proton-proton running will allow measurements focusing on constraining the gluon polarization towards smaller Bjorken-x values. The actual longitudinal double-spin asymmetries are much smaller compared to the 200GeV program due to the smaller gluon polarization at smaller Bjorken-x values. The projected uncertainties for inclusive jet production are shown in Figure 4.19 as a function of x_T. Figure 4.20 shows the projected performance for four different pseudo-rapidity combinations for di-jet production. These measurements would extend previous

measurements into the lower Bjorken-x region. The case for di-jet production has been discussed in detail previously for the Run 9 BUR for $\sqrt{s}$ = 200 GeV running.

Figure 4.20: Projected A_{LL} for di-jet production for a large, multi-year, 500GeV data sample as function of the di-jet invariant mass M for different pseudo-rapidity regions.

Following a successful development of RHIC luminosity and polarization performance during Run 11, including reproducible delivery of beams with 50% polarization or more for physics at STAR, we propose to use 10 weeks of polarized proton running in Run 12 to start the above multi-year $\sqrt{s}$ = 500 GeV spin physics program. In this scenario, we would aim to return to and complete the spin physics program at $\sqrt{s}$ = 200 GeV in the subsequent running period with polarized protons.

4.6. Spin Physics at $\sqrt{s}$ = 200 GeV

The beam use proposal as outlined in the previous sections does not foresee the return to and completion of the $\sqrt{s}$ = 200 GeV spin physics program in Run 11 and Run 12, provided that proton beam polarizations of 50% or more, at the high end of or exceeding the RHIC Collider Projections, are achieved routinely and reproducibly during physics production running towards the end of Run 11.

In this scenario, we propose to return to and complete the longitudinal and transverse spin physics program at $\sqrt{s}$ = 200 GeV, as described in detail in our Beam Use Proposal for Run 9 [6], in the next polarized proton run following Run 12. As described in section 4.2, the acquired FoM with longitudinal beam polarizations at $\sqrt{s}$ = 200 GeV at the end of Run 9 fell short of the needed FoM by a factor of about three and no data were acquired with transverse beam polarizations. Among the main physics drivers for the Run 9 measurements were (the start of) measurements of coincident photon and away-side jet production in transversely polarized proton collisions at $\sqrt{s}$ = 200 GeV, as well as precision measurements of inclusive jet production beam-spin asymmetries with longitudinally polarized proton beams, di-jet A_{LL}, and γ+jet A_{LL}. We consider each of these goals to be of continued high priority. At the time of writing this proposal, data production for Run 9 is near completion and significant progress has been made to wards assessing realistic efficiencies and purities for the γ+jet A_{LL} measurement. We will report on these and on analysis progress in a future beam-use proposal.

References

[1] B.I. Abelev *et al,* (STAR collaboration), Phys. Rev. Lett. **101**, 222001(2008).
[2] P.M. Nadolsky and C.P. Yuan, Nucl. Phys. **B666**, 31(2003).
[3] D. deFlorian and W. Vogelsang, hep-ph/1003.4533.
[4] D. deFlorian, G.A. Navarro and R. Sassot, Phys. Rev. **D71**, 094018(2005).
[5] D. deFlorian *et al,* Phys. Rev. Lett. **101**, 072001(2008).
[6] http://www.bnl.gov/npp/docs/pac0508/STAR_BUR_21April08.pdf